Boundary conditions at fluid porous interfaces

Christian Ruyer-Quil, Sanghasri Mukhopadhyay, R Usha

Boundary conditions at fluid porous interfaces

Christian Ruyer-Quil[1], Sanghasri Mukhopadhyay[2], and R Usha[3]

[1]Université Savoie Mont Blanc, CNRS, LOCIE, 73000 Chambéry, France
[2]TDepartment of Mathematics, School of Advanced Sciences, Vellore Institute of Technology, Vellore 632014, Tamil Nadu, India
[3]Department of Mathematics, IIT Madras, Chennai, 600036 Tamil Nadu, India.

Abstract

We derive boundary conditions at the interface of a homogeneous and isotropic porous medium and an overlying fluid layer by averaging the generalized transport equations in the interfacial region and rewriting the obtained jump conditions at the effective sharp interface dividing the homogeneous fluid and porous layers, thus taking into account the thickness of the diffuse interface. We obtained jump boundary conditions in terms of geometrical parameters, namely the Brinkman penetration depth δ_B, the ratio $a = \Delta/\delta_B$ of the thickness of the interfacial region to the Brinkman depth, and the location of the effective dividing interface. This is the first attempt to determine the appropriate location of the diving interface by matching the solutions to the one-domain and two-domain approaches. Jump boundary conditions reduce to the slip-transpiration-resistance model proposed by Lācis *et al.* [29], either in the thick interface limit ($e^a \gg 1$) or if the Darcy law is assumed to apply in the porous medium. In these limits, adequate choice of the dividing interface location enables to replace the slip condition by the continuity of the tangential velocity, yielding a simpler Dirichlet-transpiration-resistance model. Our formulation has the advantage that the effective coefficients depend explicitly on geometrical parameters that are easy to estimate in practice and, therefore, can be easily implemented. Numerical tests for parallel and non-parallel flows using the obtained boundary conditions or the generalized transport equations show excellent agreement. Our results can be easily extended to deal with 3D configurations and anisotropic porous media.

Keywords: porous media, flow-structure interaction

1 Introduction

One of the long-standing sources of challenging problems for mathematical analysis is the description and modelling of transport phenomena of a fluid in a porous medium and the transitional region at a fluid-porous interface responsible for mass and momentum transfer. The necessity for addressing this problem stems not only from the significant influence exerted by the presence of small-scale surface inhomogeneities at the interface on the transport phenomena but also from its ubiquitous occurrence in nature (benthic boundary layer, turbulent flow in the forest or urban location, flows over gravel stream beds, contaminant transport in rivers or atmosphere) and in many industrial and environmental applications (dendritic solidification of multicomponent mixtures, oil recovery, flow in heat exchangers, fuel cell and separation processes, in nuclear reactor vessels, in nuclear waste repositories), see, e.g., Alazmi & Vafai [1], Angot *et al.* [4], Bottaro [7], Gavrilov *et al.* [16], Lyubimova *et al.* [33]. Starting from the pioneering study by Beavers & Joseph [6] who considered a Poiseuille flow over a permeable medium employing an empirical slip boundary condition, referred to as the Beavers and Joseph (B-J) condition, where the governing equations in the two regions (Stokes and the Darcy equations) which model the dynamics are of different differential orders, there have been several theoretical and experimental efforts in the past few decades (see Angot *et al.* [3] for details). These studies have provided different models describing the dynamics to be employed in the two regions, depending on the phenomenon to be examined, namely Darcy, Forchheimer, or Darcy-Brinkman models, and the appropriate boundary conditions needed to connect the transport models in the two regions, so that one can investigate the dynamics in the whole region, determine and quantify the role

of the interfacial region. The B-J jump condition contains a dimensionless slip coefficient that depends on the microstructure of the interfacial region [6, 17, 36, 40, 43, 45, 49, 50, 54]. Note that the transition region is one in which the flow velocity in the fluid layer reduces drastically until it reaches an average seepage velocity that the Darcy equation can predict. It is crucial to examine the general form of the admissible boundary conditions from a mathematical point of view, given the models in the fluid and the porous regions. It is also important to characterize the transfer in the transition region (mass, momentum) and to model these by appropriate boundary conditions.

From a macroscopic perspective (where the concept of interface is related to the average representation), the fluid flow in a coupled flow system has been characterized by two modelling approaches, the One-Domain Approach (ODA) and the Two-Domain Approach (TDA), which employ volume-averaging techniques that provide a framework for obtaining macroscopic models from point-wise models at fluid and porous medium scales [49].

The ODA considers the system as a continuum, where the geometrical properties (porosity, permeability) and transport phenomena display rapid spatial changes in the inter-region [17, 36, 46, 49, 50], regarded as a thin transition porous layer (see figure 1 a). The earlier attempts to describe the transport governed by the generalized transport equations (GTE), valid everywhere in the entire system, have employed heuristic expressions for permeability, but the predictions near the interface have not been satisfactory [14, 25]. This suggested a need for accounting for the correct spatial dependence of permeability everywhere in the system through the GTE and for understanding how the spatial variations of the effective coefficients are related to the size of the averaging volume employed to derive the macroscopic equations. The subsequent efforts to fulfil the above requirements are based on GTE formulations, which are free of length constraints, and they accounted for porosity variations by including first and second Brinkman correction terms [39, 48]. There were suggestions to neglect the second Brinkman correction term [11, 12, 13] as its contribution is considered through the other terms in the GTE. However, the inclusion of these terms has also been accepted as it can be regarded just as a result of the up-scaling method employed to derive the macroscopic equations.

Motivated by the relevance of the derivation of a reliable GTE that accurately describes the momentum transport across fluid-porous medium, Hernandez-Rodriguez *et al.* [20] have presented a momentum GTE (ODA approach), valid everywhere in the system and expressed in terms of position-dependent effective medium coefficients, containing the two Brinkman corrective terms along with the Darcy term. The ODA predictions compare well with the results generated by averaging the local profiles resulting from pore-scale simulations. They have predicted the position-dependent permeability tensor from both pore-scale simulations and the solution of the corresponding local closure problem in a typical domain of the fluid-porous medium boundary. Their analysis reveals that including the first and the second Brinkman correction terms, along with the position-dependent intrinsic permeability tensor in the Darcy term in the GTE for momentum transport, facilitates accurate predictions of the average velocity profiles everywhere in the system. It is worth mentioning that the derivation of the GTE for momentum transport also gains significance in the context of TDA since one can assess whether or not the inclusion of additional terms helps in the accurate prediction of the associated jump coefficients and the position of the dividing surface.

The TDA considers the porous medium-fluid region as two continuous regions separated by a dividing surface (see figure 1 b). Different models for the fluid and the porous medium scales have been implemented and matched through the corresponding developed jump conditions at the dividing surface [51, 52]. The solution of the associated closure problems has supplied the coefficients involved in the jump conditions. There have been continued efforts in proposing adequate boundary conditions at the interface of the two domains, but there are certain features of the momentum and the mass transport phenomena that have not been accounted for, resulting in some failure to capture significant physical characteristics of the porous surface. The derivation of the boundary conditions must incorporate a direct correlation between the microscopic geometrical details of the porous medium and the corresponding macroscopic transport of mass and momentum; this being a complicated effort in such multi-scale problems, an effective approach has been proposed to capture the averaged effect of the microscale characteristics on the macroscopic processes within the framework of TDA. This corresponds to imposing the boundary conditions at a fictive interface between the free fluid and the porous region. Note that the jump boundary conditions are a result of the integration of the momentum transport over a thin transition layer of the ODA [19, 47].

The investigations devoted to the derivation of the jump boundary conditions for inertia-less, one-

dimensional channel flow parallel to the porous layer [6, 9, 19, 26, 34, 39, 42, 47], for general two or three-dimensional inertia-less viscous flow and arbitrary flow direction at the interface [3], employing asymptotic modelling [2], for inertial flow through a permeable interface [37], for multidimensional arbitrary flow direction and for macroscopic scale for one-dimensional (1D) channel flow [22, 43], at the pore scale for 1D channel flow [5, 8, 28, 32, 41, 53, 55], reveal that the jump boundary conditions represent the integration of transport phenomena over the transition layer. The derived jump boundary conditions based on the combination of the ODA and the TDA approaches have either assumed the volume averaging method [38, 39], or are based on the solution of an ancillary closure problem related to macroscopic deviations [47], or used matched asymptotic expansion [13], or asymptotic analysis [3].

In the above investigations, the normal free-flow velocity v^l is either set to zero at the interface (while modelling a porous surface with very small permeability by a rigid surface with wall slip, characterized by a slip length) or to the velocity in the porous medium justified by conservation of mass arguments or leading order boundary condition [27, 30, 35]. However, the mass transfer to the exterior fluid takes place due to stream-wise variation of the slip velocity across a depth below the interface where wall-normal velocity exists and is non-zero. Hence, the boundary condition on the wall-normal velocity at the interface must be a relation connecting v^l, the Darcy seepage velocity v^p, and the amount of exchange of mass that the porous medium permits across the interface.

Further, the free fluid pressure p^l is assumed to be continuous across the interface and is the same as the pressure in the porous medium (p^p, the pore pressure) in contrast to the theoretical and numerical predictions [24, 28, 31] which revealed that there is a jump in pressure: $p^l - p^p = 2\mu v_y$; μ is the dynamic viscosity of the fluid. Note that $v_y = 0$ stands only for parallel flows and that there are systems (non-parallel flows) such as the turbulent channel flow [29, 54] in which the wall-normal velocity fluctuations contribute to the friction at a rough/porous wall. [29] thus proposed to introduce a resistance coefficient which quantifies the friction induced by the crossing of the interface, as well as a transpiration length which represents the distance from the interface below which the normal velocity differs from the seepage Darcy one.

In such scenarios, one has to account for not only the transport of the interface tangential momentum but also that of mass and interface normal momentum. Hence, the pressure boundary condition must relate the normal stress of the free fluid flow on the interface, taking into consideration that $v_y \neq 0$ and the contribution of the frictional force generated by the Darcy seepage velocity v^p in the normal stress from the porous medium. The idea is to derive a boundary condition with a flow direction that is neither normal nor tangential to the porous fluid interface and besides is evolving in the tangential direction ($v_y \neq 0$).

The above-mentioned investigations and arguments demonstrate that the description of the transport phenomena across the transition region must accurately account for the dependence of the exchange of mass, momentum, energy, and other passive scalars on the inhomogeneities at the interface between the free-flowing fluid and the porous medium and that, for the given physical phenomena, the precise location of the interface inside the fluid-porous transitional region may have a significant impact on the final result. This suggests that it is important to propose the exact location of the interface and the appropriate boundary conditions at a sharp interface within the interfacial region, taking into account the thickness of the transitional region. The above requirement is also supported by experimental observations on transition layer thickness at a fluid, porous interface in packed beds by [17]. The thickness 2Δ of the transition zone (height below the permeable interface up to which the velocity decreases to the Darcy seepage velocity) has been shown to be of the order of the grain diameter and hence much larger than the square root of the permeability.

This calls for the derivation of appropriate boundary conditions at a sharp interface within the transitional region of the thickness of order 2Δ, i.e. of the order of the grain diameter, employing accurate quadrature rules to evaluate the integrals involved in the computations. In view of the above, the present study considers the derivation of the jump boundary conditions at a fluid-porous medium interface (TDA), taking into account the transitional layer thickness and integrating the ODA governing equations across the diffuse interface employing consistent quadrature rules [3].

In our geometrical argument, we take into account the following two effects within the TDA: (i) the effect of the transition between the fluid and the porous region and (ii) the Brinkman diffusion within the bulk of the porous medium. Note that if the Brinkman sub-layer, defined as the region of the flow where Brinkman diffusive terms are non-negligible, is included within the interfacial region, it makes no sense

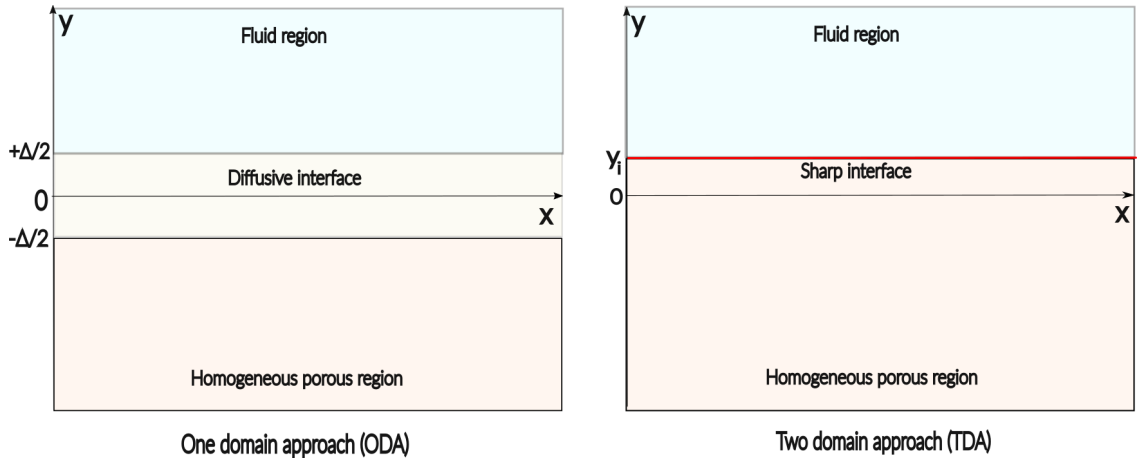

Figure 1: Sketches of the interfacial fluid-porous interfacial region modelled by the ODA, TDA approaches.

to include Brinkman corrections in the bulk of the porous medium within the framework of TDA. Thus, it is more appropriate to use the Darcy approximation of the porous flow coupled with the jump boundary conditions. In this regard, we have identified two parameters that characterize the interfacial region, namely, the thickness of the interfacial region, Δ and the ratio $a = \Delta/\delta_B$ of interfacial thickness to the Brinkman penetration depth δ_B (the depth below which the Brinkman diffusive terms are dominant), and propose to present the appropriate boundary conditions for the TDA. We have obtained sets of boundary conditions that are expressed explicitly in terms of these two parameters, in contrast to the previous attempts where the coefficients in the boundary conditions are given in terms of the integrals of the pore-scale variables.

The paper is organized as follows: Section 2 presents the mathematical description of the proposed model and the derivation of the effective homogenized boundary conditions, with coefficients expressed explicitly in terms of the three relevant parameters introduced. The proposed TDA model is validated for channel flow and stagnation point flow over a porous wall with the suction flow in section 3, and section 4 presents the concluding remarks.

2 Mathematical modelling

We consider a system comprising fluid and porous regions separated by a planar diffuse interface at $y = 0$, of thickness $2\bar{\Delta}$. The porous bed is isotropic and homogeneous, i.e., the permeability and porosity in the bulk of the porous region are assumed constant, κ_H and ε_H, and to vary continuously as functions $\kappa(y)$ and $\varepsilon(y)$ within the diffuse interfacial region. Fundamental properties of the fluid, density (ρ) and dynamic viscosity (μ) are considered to remain constant. The kinematic viscosity is denoted by $\nu = \mu/\rho$. For ease of simplicity, we limit ourselves to considering a two-dimensional (2D) flow, though the analysis can be generalized to 3D flows without difficulty.

Within the one-domain approach (ODA) (for details see Hernandez-Rodriguez *et al.* [20], Hirata *et al.* [23]), the flow is governed by the equations

$$\nabla \cdot \mathbf{v} = 0, \tag{1a}$$

$$\frac{Re}{\varepsilon}\left[\mathbf{v}_t + \nabla\cdot\left(\frac{1}{\varepsilon}\mathbf{v}\otimes\mathbf{v}\right)\right] = -\nabla p + \frac{1}{\varepsilon}\Delta\mathbf{v} - \frac{1}{\kappa}\mathbf{v} - \frac{1}{\varepsilon}\nabla\varepsilon\cdot\nabla\left(\frac{\mathbf{v}}{\varepsilon}\right). \tag{1b}$$

where subscripts denote partial derivatives. Body forces, such as gravity, are here assumed to derive from a potential and are included in the definition of the pressure field. The last terms $-\varepsilon^{-1}\nabla\varepsilon\cdot\nabla\left(\varepsilon^{-1}\mathbf{v}\right)$ are the second Brinkman corrections, which are non-zero only in the diffuse interfacial regions where the porosity gradients cannot be a priori neglected. However, these terms are generally considered to be weak, though Hernandez-Rodriguez *et al.* [20] have shown that they must be retained in order to capture precisely the

velocity profile of parallel flows. As shown later on in this work, these terms affect only weakly the base flow profile. We will therefore neglect them in our analysis of the interfacial region.

The governing equations have been made dimensionless using characteristic length $\bar{L}$ and velocity $\bar{U}$ scales, e.g. the total thickness of the entire continuum and the averaged velocity of the fluid. The pressure scale is equal to $\mu\bar{U}/\bar{L}$. Three dimensionless groups characterize the flow, namely the Reynolds number $Re = \bar{U}\bar{L}/\nu$, the Darcy number $Da = \kappa_H/\bar{L}^2$ and the dimensionless thickness of the interfacial region $\Delta = \bar{\Delta}/\bar{L}$.

In contrast, within the two-domain approach (TDA), the porous and fluid domains are separated by a sharp interface of zero thickness, the fluid and porous regions being homogeneous. Within TDA, the location y_i of the sharp interface dividing the fluid and porous regions can be chosen arbitrarily within the interfacial region, i.e. $-\Delta < y_i < \Delta$. The solution to the TDA, labelled with l and p superscripts, is governed by the Navier-Stokes equation in the liquid phase

$$\nabla\cdot\mathbf{v}^l = 0\,, \quad Re\left[\mathbf{v}^l_t + \nabla\cdot\left(\mathbf{v}^l\otimes\mathbf{v}^l\right)\right] = -\nabla p^l + \Delta\mathbf{v}^l\,, \tag{2}$$

and the Darcy-Brinkman equations

$$\nabla\cdot\mathbf{v}^p = 0\,, \quad 0 = -\nabla p^p + \frac{1}{\varepsilon_H}\Delta\mathbf{v}^p - \frac{1}{Da}\mathbf{v}^p\,, \tag{3}$$

or the Darcy equations

$$\nabla\cdot\mathbf{v}^p = 0\,, \quad 0 = -\nabla p^p - \frac{1}{Da}\mathbf{v}^p\,, \tag{4}$$

if the first Brinkman correction is neglected or not in the porous phase.

2.1 Interfacial jump conditions

Following [3], we integrate the ODA governing equations (1) across the diffuse interfacial region in order to obtain jump conditions connecting the fluid and porous layers. We introduce the scale $\delta_B = \sqrt{Da/\varepsilon_H}$ below which Brinkman diffusive terms are dominant in the bulk of the porous medium. We will thus refer to δ_B as a Brinkman penetration depth.

Noteworthy is that our definition of the Brinkman penetration depth differs from the thickness of the Brinkman boundary layer, which we denote here by Δ_B, as identified by Hernandez-Rodriguez *et al.* [21] as the typical distance over which the velocity profile decreases drastically from the velocity at the surface of the porous medium to the Darcy seepage velocity. These authors have shown that the extension of this boundary layer is of the order of the size r_0 of the averaging volume in the homogenization method, which also corresponds to the typical extension of the variations of the permeability distribution obtained by the same method [20]. Thus $\Delta_B = O(\Delta)$, and may be much larger than the Brinkman penetration depth δ_B in their computations. We thus infer that the Brinkman boundary layer has a thickness Δ_B of the order of the maximum of δ_B and Δ.

As the interfacial region is thin in comparison to the macro scale, we stretch the normal coordinate as $Y = y/\Delta$. The continuity equation thus reads

$$\Delta u_x + v_Y = 0 \tag{5}$$

Since $u_x = O(1)$ and, in the bulk of the porous region, the velocity is governed by the Darcy law, i.e. $v = O(Da) = O(\delta_B^2) = O(\Delta^2/a^2)$, we conclude that $v = O(\Delta)$ in the interfacial region. We thus rescale the normal velocity component such that $V = v/\Delta$.

The governing equations (1) then read

$$V_Y = -u_x\,, \tag{6a}$$

$$\frac{1}{\varepsilon}u_{YY} - \Delta^2\frac{u}{\kappa} = \Delta^2\frac{Re}{\varepsilon}\left[u_t + \left(\frac{u^2}{\varepsilon}\right)_x + \left(\frac{uV}{\varepsilon}\right)_Y\right] + \Delta^2 p_x - \frac{\Delta^2}{\varepsilon}u_{xx}\,, \tag{6b}$$

$$\frac{1}{\varepsilon}V_{YY} - \Delta^2\frac{V}{\kappa} = \Delta^2\frac{Re}{\varepsilon}\left[V_t + \left(\frac{uV}{\varepsilon}\right)_x + \left(\frac{V^2}{\varepsilon}\right)_Y\right] + p_Y - \frac{\Delta^2}{\varepsilon}V_{xx}\,, \tag{6c}$$

where $\Delta^2/\kappa = O(1)$. Truncating at order Δ, we obtain a set of equations that we rewrite with the original scales

$$v_y = -u_x\,, \tag{7a}$$

$$\frac{1}{\varepsilon}u_{yy} - \frac{u}{\kappa} = 0\,, \tag{7b}$$

$$\frac{1}{\varepsilon}v_{yy} - \frac{v}{\kappa} = p_y \tag{7c}$$

Thus, at the leading order, inertia is negligible in the interfacial region. The pressure gradient is oriented orthogonally to the interface and drives a flow in the normal direction.

Following [3], we integrate (7) using the trapezoidal quadrature rule

$$\int_a^b f(x)dx = \frac{h}{2}[f(a)+f(b)] + O\left[\max_{x\in[a,b]}|f''(x)|h^3\right] \tag{8}$$

where $h = b-a$, and the quadrature of the integral of products

$$\int_a^b f(x)g(x)dx = \frac{1}{h}\int_a^b f(x)dx\int_a^b g(x)dx + O\left[\max_{x\in[a,b]}|g'(x)|\langle|g|\rangle h^2\right]\,, \tag{9}$$

with $\langle|g|\rangle = h^{-1}\int_a^b|g|dx$.

Therefore, integration of the continuity equation (7a) gives

$$v|_\Delta - v|_{-\Delta} = -\int_{-\Delta}^{\Delta} u_x dy \approx -\Delta\,(u_x|_\Delta + u_x|_{-\Delta}) = \Delta\,(v_y|_\Delta + v_y|_{-\Delta})\,, \tag{10}$$

Similarly, we have

$$\int_{-\Delta}^{\Delta}\frac{1}{\varepsilon}u_{yy}dy \approx \frac{1}{2\Delta}\int_{-\Delta}^{\Delta}\frac{1}{\varepsilon}dy\int_{-\Delta}^{\Delta}u_{yy}dy \approx \frac{1}{2}\left(1+\frac{1}{\varepsilon_H}\right)(u_y|_\Delta - u_y|_{-\Delta}) \tag{11}$$

and

$$\int_{-\Delta}^{\Delta}\frac{u}{\kappa}dy \approx \Delta\left(\frac{u}{\kappa}|_{y=-\Delta} + \frac{u}{\kappa}|_{y=\Delta}\right) \approx \frac{\Delta}{Da}u|_{-\Delta} \tag{12}$$

We thus obtain

$$\frac{1+\varepsilon_H}{2\varepsilon_H}(u_y|_\Delta - u_y|_{-\Delta}) = \frac{\Delta}{Da}u|_{-\Delta}\,, \tag{13}$$

We next integrate the normal momentum balance (7c) to obtain

$$p|_\Delta - p|_{-\Delta} = \frac{1+\varepsilon_H}{2\varepsilon_H}(v_y|_\Delta - v_y|_{-\Delta}) - \frac{\Delta}{Da}v|_{-\Delta}\,, \tag{14}$$

To complete our system of jump conditions connecting the fluid and porous layers, we need to write a relation between the jump of velocity and the shear stress. Still following [3], we write

$$\int_{-\Delta}^{\Delta}\frac{1}{\varepsilon}u_y dy \approx \frac{1}{2\Delta}\int_{-\Delta}^{\Delta}\frac{1}{\varepsilon}dy\int_{-\Delta}^{\Delta}u_y dy \tag{15}$$

Applying the trapezoidal rule (8) on each side of this equation gives

$$\frac{1+\varepsilon_H}{2\varepsilon_H}(u|_\Delta - u|_{-\Delta}) = \Delta\left(u_y|_\Delta + \frac{1}{\varepsilon_H}u_y|_{-\Delta}\right) \tag{16}$$

Let us stress that we have computed the integrals $\int_{-\Delta}^{\Delta}u/\kappa dy$ and $\int_{-\Delta}^{\Delta}v/\kappa dy$ using the trapezoidal rule (8) instead of the quadrature rule (9) employed by Angot *et al.* [3]. As discussed in the appendix A, using (9) leads to $u|_\Delta = O(\Delta) \ll 1$, which erroneously implies that the fluid layer essentially sees a no-slip boundary

condition at the top of the interfacial region and therefore that the extension of the Brinkman boundary layer is negligible. We note that, contrary to (58a), the jump of the tangential shear stress (13) is naturally balanced as $u_y|_\Delta - u_y|_{-\Delta} = O(\Delta)$ and $u|_{-\Delta} = O(Da/\varepsilon_H)$ since the flow in the bulk of the porous medium is essentially governed by the Darcy law.

In order to obtain a set of symmetrical jump relations for the tangential and normal velocities, we rewrite the normal velocity jump by evaluating the integral $\int_{-\Delta}^{\Delta} v_y/\varepsilon dy$, which gives

$$\frac{1+\varepsilon_H}{2\varepsilon_H}\left(v|_\Delta - v|_{-\Delta}\right) = \Delta\left(v_y|_\Delta + \frac{1}{\varepsilon_H}v_y|_{-\Delta}\right) \tag{17}$$

Finally, we write a jump relation for the gradient of pressure that will be used to close the system of equations for the boundary conditions that we will derive in the next section. Taking the divergence of the momentum balance gives

$$p_{yy} = v_{yy}\frac{d}{dy}\left(\frac{1}{\varepsilon}\right) - v\frac{d}{dy}\left(\frac{1}{\kappa}\right) \tag{18}$$

which we integrate across the interfacial region as

$$\int_{-\Delta}^{\Delta} p_{yy}\,dy = \left[\frac{d}{dy}\left(\frac{1}{\varepsilon}\right)v_y - \frac{v}{\kappa}\right]_{-\Delta}^{\Delta} - \int_{-\Delta}^{\Delta}\frac{d^2}{dy^2}\left(\frac{1}{\varepsilon}\right)v_y - \frac{1}{\kappa}v_y\,dy \tag{19}$$

which gives

$$p_y|_\Delta - p_y|_{-\Delta} = \frac{1}{Da}\left(v|_{-\Delta} - \Delta v_y|_{-\Delta}\right) \tag{20}$$

which, with the help of (7c), can also be rewritten as

$$v_{yy}|_\Delta - \frac{1}{\varepsilon_H}v_{yy}|_{-\Delta} = -\frac{\Delta}{Da}v_y|_{-\Delta} \tag{21}$$

Next, we integrate v_{yy}/ε to get

$$\frac{1+\varepsilon_H}{2\varepsilon_H}\left(v_y|_\Delta - v_y|_{-\Delta}\right) = \Delta\left(v_{yy}|_\Delta + \frac{1}{\varepsilon_H}v_{yy}|_{-\Delta}\right). \tag{22}$$

The jump relations (21) and (22) will be used to eliminate the second derivatives of the normal velocity v and close our set of boundary equations as discussed in the next section.

The set of four jump conditions (13), (16), (14) and (17), is similar to the one derived by [3]. However, these authors postulated u_x to be negligible, and thus also v_y, and therefore found the normal velocity to be continuous within the interfacial region instead of the jump condition (17).

2.2 Two-domain approach boundary conditions

In this section, we propose to derive from the jump conditions (13), (14), (16), (17), (21) and (22), boundary conditions for the two-domain approach (TDA). We assume that the solution to the TDA, labelled with l and p superscripts to denote the fluid and porous regions, coincides with the ODA solution outside the diffuse interface. Similarly to section 2.1, considering the diffuse interface to be thin, a boundary-layer analysis gives at leading order

$$v_y^p = -u_x^p\,, \quad \frac{1}{\varepsilon_H}u_{yy}^p - \frac{u^p}{Da} = 0\,, \quad \frac{1}{\varepsilon_H}v_{yy}^p - \frac{v^p}{Da} - p_y^p = 0\,, \tag{23a}$$

$$v_y^l = -u_x^l\,, \quad u_{yy}^l = 0\,, \quad v_{yy}^l - p_y^l = 0\,. \tag{23b}$$

Taking the divergence of the momentum balances gives Laplace equations for the pressure field, i.e.

$$p_{yy}^l = 0\,, \qquad p_{yy}^p = 0\,, \tag{24}$$

from which we deduce that the pressure gradients p^l_y and p^p_y are independent of y at leading order within the interfacial region. Matching with the outer regions thus ensures that p^l_y and p^p_y are $O(1)$ quantities and therefore, $v^p = O(\Delta^2)$, $v^p_y = O(\Delta)$, $v^p_{yy} = O(1)$, $v^l = O(\Delta^2)$, $v^l_y = O(\Delta)$ and $v^l_{yy} = O(1)$. Consequently, the continuity equations provide the estimates $u^p = O(\Delta)$, $u^p_y = O(1)$, $u^l = O(\Delta)$, $u^l_y = O(1)$ within the interfacial region. These ordering relations will be used to discuss the boundary conditions which we propose below.

From (23), the tangential velocity component can easily be integrated to give

$$u^p = u^p|_i \cosh\frac{y-y_i}{\delta_B} + \delta_B u^p_y|_i \sinh\frac{y-y_i}{\delta_B}\,, \qquad u^l = u^l|_i + (y-y_i)u^l_y|_i \tag{25a}$$

From which the normal velocity component can be obtained with the help of the continuity equation

$$v^p = v^p|_i + v^p_y|_i\delta_B \sinh\frac{y-y_i}{\delta_B} + v^p_{yy}|_i\delta_B^2\left[\cosh\frac{y-y_i}{\delta_B} - 1\right], \qquad v^l = v^l|_i + (y-y_i)\,v^l_y|_i + \frac{(y-y_i)^2}{2}v^l_{yy}|_i\,, \tag{25b}$$

and the pressure distribution

$$p^p = p^p|_i + (y-y_i)\left(\frac{1}{\varepsilon_H}v^p_{yy}|_i - \frac{v^p|_i}{Da}\right), \qquad p^l = p^l|_i + (y-y_i)\,v^l_{yy}|_i \tag{25c}$$

Substitution of (25) into (13) and (16) leads to the following boundary conditions expressed at the sharp interface $y = y_i$:

$$\begin{aligned}
p^l|_i - p^p|_i &= \frac{\xi}{\delta_B\varepsilon_H}v^p|_i + \frac{1+\varepsilon_H}{2\varepsilon_H}v^l_y|_i - \alpha v^p_y|_i + (\xi+\gamma)\delta_B v^l_{yy}|_i \\
&\quad + \left(\beta - \frac{\xi}{\varepsilon_H}\right)\delta_B v^p_{yy}|_i\,, && \text{(26a)}\\
\frac{1+\varepsilon_H}{2\varepsilon_H}u^l_y|_i - \alpha\, u^p_y|_i &= -\frac{\beta}{\delta_B}u^p|_i\,, && \text{(26b)}\\
\frac{1+\varepsilon_H}{2\varepsilon_H}u^l|_i - \alpha\, u^p|_i &= -\gamma\delta_B u^l_y|_i - \beta\,\delta_B u^p_y|_i\,, && \text{(26c)}\\
\frac{1+\varepsilon_H}{2\varepsilon_H}\left(v^l|_i - v^p|_i\right) &= -\gamma\delta_B v^l_y|_i - \beta\,\delta_B v^p_y|_i + \zeta\,\delta_B^2 v^l_{yy}|_i + \delta_B^2\left(\alpha - \frac{1+\varepsilon_H}{2\varepsilon_H}\right)v^p_{yy}|_i\,, && \text{(26d)}\\
v^l_{yy}|_i - \hat\alpha v^p_{yy}|_i &= -\frac{\hat\beta}{\delta_B}v^p_y|_i\,, && \text{(26e)}\\
\frac{1+\varepsilon_H}{2\varepsilon_H}v^l_y|_i - \alpha\, v^p_y|_i &= -\gamma\delta_B v^l_{yy}|_i - \beta\,\delta_B v^p_{yy}|_i\,, && \text{(26f)}
\end{aligned}$$

where $\xi = y_i/\delta_B$ and

$$\begin{aligned}
\alpha &= \frac{(1+\varepsilon_H)C - 2aS}{2\varepsilon_H}\,, \quad \beta = \frac{(1+\varepsilon_H)S - 2aC}{2\varepsilon_H}\,, \quad \gamma = \frac{(a-\xi)(1-\varepsilon_H)}{2\varepsilon_H} - \xi\,, && \text{(27a)}\\
\zeta &= \frac{(a-\xi)[\xi(1+\varepsilon_H) + a(3\varepsilon_H - 1)]}{4\varepsilon_H}\,, && \text{(27b)}\\
\hat\alpha &= \frac{C + aS}{\varepsilon_H}\,, \quad \hat\beta = \frac{S + aC}{\varepsilon_H}\,, && \text{(27c)}\\
C &= \cosh(a+\xi)\,, \quad S = \sinh(a+\xi)\,, \quad \text{and} \quad a = \Delta/\delta_B\,. && \text{(27d)}
\end{aligned}$$

Differentiating (26b) and (26c) with respect to x and adding them to (26d) and (26a) gives

$$\begin{aligned}
p^l|_i - p^p|_i &= \frac{\xi}{\delta_B\varepsilon_H}v^p|_i + \xi\,\delta_B\left(v^l_{yy}|_i - \frac{1}{\varepsilon_H}v^p_{yy}|_i\right), && \text{(28a)}\\
\frac{1+\varepsilon_H}{2\varepsilon_H}\left(v^l|_i - v^p|_i\right) &= -\gamma\delta_B v^l_y|_i + \delta_B^2\left(\zeta + \frac{1+\varepsilon_H}{2\varepsilon_H}\right)v^l_{yy}|_i - \delta_B^2\frac{1+\varepsilon_H}{2\varepsilon_H}v^p_{yy}|_i && \text{(28b)}
\end{aligned}$$

Combining (26e) and (26f) enables to eliminate $v^l_{yy}|_i$ and $v^p_{yy}|_i$, which leads to the boundary conditions

$$p^l|_i - p^p|_i = \frac{\xi}{\delta_B \varepsilon_H} v^p|_i - \xi \left(\phi v^l_y|_i + \psi v^p_y|_i \right), \tag{29a}$$

$$\frac{1+\varepsilon_H}{2\varepsilon_H} u^l_y|_i - \alpha u^p_y|_i = -\frac{\beta}{\delta_B} u^p|_i, \tag{29b}$$

$$\frac{1+\varepsilon_H}{2\varepsilon_H} u^l|_i - \alpha u^p|_i = -\gamma \delta_B u^l_y|_i - \beta \delta_B u^p_y|_i, \tag{29c}$$

$$v^l|_i - v^p|_i = -\hat{\phi} \delta_B v^l_y|_i - \hat{\psi} \delta_B v^p_y|_i. \tag{29d}$$

where

$$\phi = \frac{(1+\varepsilon_H)(\hat{\alpha}\varepsilon_H - 1)}{2\varepsilon_H^2(\beta + \hat{\alpha}\gamma)}, \tag{30a}$$

$$\psi = \frac{\alpha(1-\hat{\alpha}\varepsilon_H) + \hat{\beta}(\beta\varepsilon_H + \gamma)}{\varepsilon_H(\beta + \hat{\alpha}\gamma)}, \tag{30b}$$

$$\hat{\phi} = \frac{\hat{\alpha} - (1+\varepsilon_H)^2 + 4\beta\varepsilon_H^2\gamma + \hat{\alpha}\varepsilon_H\left[2 + \varepsilon_H + 4\varepsilon_H\gamma^2 + 2(1+\varepsilon_H)\zeta\right]}{2\varepsilon_H(1+\varepsilon_H)(\beta + \gamma\hat{\alpha})}, \tag{30c}$$

$$\hat{\psi} = \frac{(1+\varepsilon_H)[\alpha(1-\hat{\alpha}) + (\beta+\gamma)\hat{\beta}] + 2(\beta\hat{\beta} - \alpha\hat{\alpha})\varepsilon_H\zeta}{(1+\varepsilon_H)(\beta + \gamma\hat{\alpha})} \tag{30d}$$

Conditions (29c) and (29d) represent the jump of velocity induced by the shear rate in the interfacial region. (29a) corresponds to the jump of pressure generated by the balance of normal stresses at the interface. Finally, (29b) accounts for the friction exerted by the porous medium on the flow in the interfacial region, which is responsible for a jump in tangential shear rate.

From (29a), we obtain that, at the leading order, the pressure is continuous if the sharp interface is chosen to correspond to the middle of the diffuse interfacial region ($\xi = 0$). This result is consistent with the pore-scale simulations of a fluid-porous interface performed by Carraro *et al.* [10] for an isotropic porous medium. However, the coefficients of the boundary conditions (29) are dependent on the choice of location of the dividing sharp interface through the parameter ξ. This calls for the best choice of that parameter, which enables to obtain the best agreement between ODA and TDA solutions. Finding the best value for ξ has no clear answer. However, since tangential velocities u^l and u^p are $O(\Delta)$ in the interfacial region, whereas the normal velocities are $O(\Delta^2)$, it is convenient to look for the value of ξ based on the tangential velocity profiles.

The Darcy seepage velocity being small, we propose to adjust ξ in order to set $u^l|_i$ to zero, or close to zero, so that $u^p|_i \approx u^l|_i$. Because of the exponential nature of the solution (25), we have $u^p|_i \approx \delta_B u^p_y|_i$. Thus, setting $u^p|_i = \delta_B u^p_y|_i$ and $u^l|_i$ into the velocity and shear stress boundary conditions (29c) and (29b) yield

$$(1 + \varepsilon_H - 2\varepsilon_H\gamma) u^l_y|_i = 0 \tag{31}$$

Since $u^l_y|_i \neq 0$, we obtain a condition for the location of the sharp interface, namely

$$\xi = \frac{a(1-\varepsilon_H) - 1 - \varepsilon_H}{1+\varepsilon_H}, \tag{32}$$

The condition $\xi > -a$ implies $a > (1+\varepsilon_H)/2$. Thus, (32) will be employed only for $a > (1+\varepsilon_H)/2$ to guarantee a location of the sharp dividing interface within the interfacial region. In the case of a thin interfacial region, for which $a < (1+\varepsilon_H)/2$, the sharp dividing interface is placed at the middle of the interfacial region ($\xi = 0$).

2.3 Thick interface limit

The thickness of the interfacial region is generally much larger than the Brinkman penetration depth, so the ratio $a = \Delta/\delta_B > 1$. This is justified by the experimental observations of Goharzadeh *et al.* [17]. Let

us thus consider the limit of a thick diffuse interface, i.e. $A = e^{-a} \ll 1$, $\cosh a \approx 1/(2A)$ and $\sinh a \approx 1/(2A)$. Expanding the boundary conditions (29c) and (29b) for the tangential velocities and shear rates and truncating them at the leading order with respect to A give

$$u^p|_i = \delta_B u_y^p|_i\,, \tag{33a}$$

$$u^l|_i = -\delta_B \frac{(1-\varepsilon_H)a + (1+\varepsilon_H)(1-\xi)}{1+\varepsilon_H} u_y^l|_i\,, \tag{33b}$$

Therefore, in the case of a thick diffuse interface, a partial decoupling of the fluid and porous regions is observed as the shear rate at the sharp interface $y = y_i$ in the fluid (porous) region depends only on the velocity in the fluid (porous) region. (33b) is the slip boundary condition obtained by [42] using homogenization techniques, starting from the Darcy equations in the porous medium [26].

We note that $a \gg 1$ implies that the diffuse interface thickness 2Δ is much larger than the Brinkman penetration depth δ_B, which is the scale below which Brinkman diffusive terms are effective. Therefore, the Brinkman diffusion is inefficient at the scale Δ and the fluid region experiences a permeable boundary essentially governed by the Darcy law. Since scales smaller or of the order of Δ are not resolved in the TDA, accounting for the Brinkman diffusive terms in the homogeneous porous region in the limit of a thick diffuse interface makes little sense. Besides, for a thick interfacial region, the exponential nature of the solution to the Darcy-Brinkman equation leads to unrealistic values of u^p. Therefore, we assume a Darcy flow in the porous medium. Because of the degeneracy of the Darcy equation, the condition (33a) cannot be enforced in that case. Besides, for a Darcy flow, (24) implies that $v_y^p \approx 0$ in the interfacial region. We thus obtain

$$u^l|_i = L u_y^l|_i\,, \tag{34a}$$

$$p^l|_i - p^p|_i = -F v^p|_i + G v_y^l|_i\,, \tag{34b}$$

$$v^l|_i - v^p|_i = M v_y^l|_i\,. \tag{34c}$$

where

$$L = -\delta_B \frac{(1-\varepsilon_H)a + (1+\varepsilon_H)(1-\xi)}{1+\varepsilon_H}\,, \quad F = -\frac{\xi}{\delta_B \varepsilon_H}\,, \tag{35a}$$

$$G = \frac{\xi(1+a)(1+\varepsilon_H)}{a^2(\varepsilon_H - 1) - (1+\varepsilon_H)(\varepsilon_H - \xi) + a[\xi - 1 + \varepsilon_H(3+\xi)]}\,, \tag{35b}$$

$$M = \delta_B \frac{M_A}{M_B}\,, \tag{35c}$$

$$\begin{aligned} M_A = {} & a^3[-1 + (2-5\varepsilon_H)\varepsilon_H] + (1+\varepsilon_H)^2(-2 + 2\varepsilon_H\xi - \xi^2) \\ & + a(1+\varepsilon_H)\{-2 + 2\varepsilon_H^2 - (\xi-2)\xi - \varepsilon_H[4 + \xi(6+\xi)]\} \\ & + a^2\{-1 + 2\xi + \varepsilon_H[6 - \varepsilon_H(9+2\xi)]\}\,, \end{aligned} \tag{35d}$$

$$M_B = 2(1+\varepsilon_H)(a + a^2 + \varepsilon_H - 3a\varepsilon_H - a^2\varepsilon_H + \varepsilon_H^2 - (1+a)(1+\varepsilon_H)\xi)\,. \tag{35e}$$

System (34) is similar to the model proposed by [29] to represent the interfacial momentum transfer at a rough or porous interface. Lācis et al. introduced a length, corresponding to the dimensionless coefficient M, which they call transpiration length, which represents the distance below which the normal velocity component differs from the Darcy seepage velocity. They also introduced a resistance coefficient F, which modelled the friction of the porous matrix on the flow in the normal direction. However, they assumed the shear stress in the fluid layer at the sharp interface to be equal to its value in the bulk of the flow, which corresponds to taking G equal to 2. Note that in our derivation, coefficients F and G are proportional to ξ. Hereinafter, we refer to (34) as the Slip-Transpiration-Resistance (STR) model.

The STR model (34) can be further simplified by conveniently choosing the location of the sharp interface such that to cancel out the slip length $L = 0$, which gives

$$\xi = \frac{1 + a + \varepsilon_H(1-a)}{1+\varepsilon_H}\,. \tag{36}$$

This choice leads to a no-slip boundary condition $u^l|_i = 0$, or more exactly to $u^l|_i = O(\Delta^2)$ as we solve the leading-order system of equations with respect to the expansion parameter Δ. Since the seepage velocity in the porous medium is $O(\Delta^2)$, we replace this no-slip condition with the continuity of the tangential velocity. Therefore, (34) is modified into

$$
\begin{aligned}
u^l|_i &= u^p|_i\,, && \text{(37a)}\\
p^l|_i - p^p|_i &= -F v^p|_i + G v^l_y|_i\,, && \text{(37b)}\\
v^l|_i - v^p|_i &= M v^l_y|_i\,, && \text{(37c)}
\end{aligned}
$$

which we refer to hereinafter as the Dirichlet-Transpiration-Resistance (DTR) model. The resistance coefficient F, the transpiration dimensionless length M and the stress coefficient G are then given by

$$
\begin{aligned}
F &= -\frac{\xi}{\delta_B \varepsilon_H} = -\frac{1+a+\varepsilon_H(1-a)}{\delta_B \varepsilon_H(1+\varepsilon_H)}\,, \quad G = \frac{1+\varepsilon_H+a[2+a(1-\varepsilon_H)]}{1-\varepsilon_H^2+a(1+3\varepsilon_H)}\,, && \text{(38a)}\\
M &= \delta_B \frac{4a^2\varepsilon_H^2(1+a)-(1+\varepsilon_H)^2(2\varepsilon_H-3)+a(3+10\varepsilon_H+7\varepsilon_H^2)}{2(1+\varepsilon_H)[1-\varepsilon_H^2+a(1+3\varepsilon_H)]}\,. && \text{(38b)}
\end{aligned}
$$

Let us underline that the no-slip boundary condition $u^l|_i = 0$ would have led to inconsistencies, as it implies that $v^l_y|_i = -u^l_x|_i = 0$. However, $v^l_y = O(\Delta^2)$ is of the same order of magnitude as $v^p|_i = O(\Delta^2)$ and must not be dropped out.

2.4 Two-domain approach boundary conditions for a Darcy flow

As stated above, the exponential nature of the solution to the TDA approach within the interfacial region leads to unreasonable values of the tangential velocity in the vicinity of the sharp interface when the boundary conditions (29) are applied, i.e. whenever $a \gtrapprox 2$ as will be shown in the next section. The conditions (37) can be employed along with the Darcy equation in the homogeneous porous medium but only if $e^a \gg 1$, which requires $a \gtrapprox 5$. Another set of boundary conditions must be derived to bridge the gap in the range $2 \lessapprox a \lessapprox 5$.

A remedy for this drawback is to assume a Darcy flow within the homogeneous porous medium in the interfacial region. Thus, the leading-order equations for the TDA approach within the interfacial region become

$$
v^p_y = -u^p_x\,, \quad \frac{u^p}{Da} = 0\,, \quad \frac{v^p}{Da} + p^p_y = 0\,. \tag{39}
$$

which gives $u^p = 0$ in the interfacial region, so that the tangential velocity is at least of order $O(\Delta^2)$. Considering a zero tangential velocity yields a too-degenerate representation of the flow. We thus assume u^p small but non-zero and introduce the ansatz

$$
u^p = u^p|_i\,, \quad v^p = v^p|_i + (y-y_i)v^p_y|_i\,, \quad p^p = p^p|_i - \frac{1}{Da}\left((y-y_i)v^p|_i + \frac{(y-y_i)^2}{2}v^p_y|_i\right) \tag{40}
$$

Thus the jump conditions (13) and (16) for the tangential velocity and shear stress yield

$$
\begin{aligned}
u^p|_i &= \frac{1+\varepsilon_H}{2a} u^l_y|_i\,, && \text{(41a)}\\
\frac{1+\varepsilon_H}{2\varepsilon_H} u^l|_i &= \left[a + \frac{(1+\varepsilon_H)(1-2a^2+\varepsilon_H+2a\xi)}{4a\varepsilon_H}\right]\delta_B u^l_y|_i\,. && \text{(41b)}
\end{aligned}
$$

The relation (41a) is degenerate as the Darcy law is of lower order than the Darcy-Brinkman law and, therefore, cannot be enforced as a boundary condition at the fluid-porous sharp interface.

Substitution in the jump conditions for the pressure gradient and the normal shear stress give

$$
\begin{aligned}
v^l_{yy}|_i &= \frac{a(1+\varepsilon_H)}{\delta_B[a^2(\varepsilon_H-1)-\varepsilon_H(1+\varepsilon_H)+a(1+\varepsilon_H)\xi]} v^l_y|_i\,, && \text{(42)}\\
v^p_y|_i &= \frac{\varepsilon_H(1+\varepsilon_H)}{a^2(1-\varepsilon_H)+\varepsilon_H(1+\varepsilon_H)-a(1+\varepsilon_H)\xi} v^l_y|_i && \text{(43)}
\end{aligned}
$$

The set of boundary conditions then reduces to the STR model (34) where

$$L = \delta_B \left[\frac{a(\varepsilon_H - 1)}{1+\varepsilon_H} + \frac{1+\varepsilon_H}{2a} + \xi \right], \quad F = -\frac{\xi}{\delta_B \varepsilon_H}, \tag{44a}$$

$$G = -\frac{(1+\varepsilon_H)(a^2 - 2a\xi - \xi^2)}{2[a^2(\varepsilon_H - 1) - \varepsilon_H(1+\varepsilon_H) + a(1+\varepsilon_H)\xi]}, \tag{44b}$$

$$M = -\delta_B a \left[\frac{a^2[1+\varepsilon_H(5\varepsilon_H - 2)] + 2a(\varepsilon_H^2 - 1)\xi + (1+\varepsilon_H)^2\xi^2}{4\varepsilon_H(a^2 + \varepsilon_H - a^2\varepsilon_H + \varepsilon_H^2 - a(1+\varepsilon_H)\xi} \right]. \tag{44c}$$

Note that, unlike (35), the expression of the coefficient G in (44) is not proportional to ξ, as a result of the dissymmetry of the pressure distributions in the fluid and porous layers introduced by the choice of the Darcy law in the interfacial region.

The slip length L can again be set to zero by adjusting the location of the sharp interface such that

$$\xi = \frac{1-\varepsilon_H}{1+\varepsilon_H} a - \frac{1+\varepsilon_H}{2a} \tag{45}$$

We thus again simplify the STR model (34) into the DTR model (37) where the coefficients F G and M are given by

$$F = -\frac{\xi}{\delta_B \varepsilon_H} = -\frac{1}{\delta_B \varepsilon_H} \left(\frac{1-\varepsilon_H}{1+\varepsilon_H} a - \frac{1+\varepsilon_H}{2a} \right), \tag{46a}$$

$$G = \frac{8a^2(1+\varepsilon_H)^2 - (1+\varepsilon_H)^4 + 8a^4[\varepsilon_H(2+\varepsilon_H) - 1]}{4a^2(1+\varepsilon_H)^2(1+3\varepsilon_H)}, \tag{46b}$$

$$M = -\delta_B \frac{1+\varepsilon_H[6 + 16a^4 + \varepsilon_H(4+\varepsilon_H)]}{4a(1+\varepsilon_H)^2(1+3\varepsilon_H)}. \tag{46c}$$

2.5 Discussion

So far, we have obtained three different formulations (29), (37) with (38), and (37) with (46), depending on the relative thickness $a = \Delta/\delta_B$ of the interfacial region with respect to the Brinkman penetration depth. For $a < 2$, the Darcy-Brinkman governing equations (3) are closed by the jump conditions (29) for the velocity, shear rate and pressure fields.

For $a > 2$, we expect the Brinkman sub-layer to be contained within the interfacial region, such that the appropriate governing equations in the porous medium are the Darcy equations (4). We obtained two similar sets of boundary conditions in that case, either by taking the limit $e^a \gg 1$ or by assuming the Darcy equations to apply within the interfacial region, which is similar to the transpiration-resistance model obtained by Lācis *et al.* [29] when written at an interface location for which the continuity of the tangential velocities replaces the Navier slip condition. However, in both cases, the resistance coefficient F is given by the same expression $F = -\xi/(\delta_B \varepsilon_H)$. Thus, the sign of F depends on the choice of the location of the sharp interface, whereas Lācis *et al.* [29] assumed it to be positive. The expression of the coefficient F can be determined rigorously, independently, without the quadrature rules employed to obtain the pressure jump condition (21) as shown in Appendix B.

3 Validation

In this section, we test the boundary conditions obtained for the TDA problem by comparing the solutions of TDA and ODA.

3.1 Channel flow

We first consider a parallel and stationary flow in a channel. The lower half of the channel is filled by a homogeneous and isotropic porous medium, and the upper half of the channel is a fluid region. The

Ratio a	**Transfer model**	**Interface location ξ**
$0 < a < \frac{1+\varepsilon_H}{2}$	Darcy-Brinkman with jump BCs (29)	$\xi = 0$
$\frac{1+\varepsilon_H}{2} < a < 2$	Darcy-Brinkman with jump BCs (29)	ξ given by (32)
$2 < a < 5$	Darcy with DTR model l(37) and (46)	ξ given by (45)
$a > 5$	Darcy with DTR model (37) and (38)	ξ given by (36)

Table 1: Summary of the different proposed representations of the mass and momentum transfer at the fluid-porous interface within the two-domain approach.

interfacial region extending from $y = -\Delta$ to $y = \Delta$ is modelled within the ODA by differentiable functions of the form

$$\varepsilon(y) = \frac{1}{2}\left[1 + \varepsilon_H + (1-\varepsilon_H)\,\mathrm{erf}\,(by)\right], \quad \frac{1}{\kappa(y)} = \frac{1}{2Da}\left[1 - \mathrm{erf}\,(by)\right], \tag{47}$$

where the constant b determines the extension Δ of the interfacial region. The channel height is denoted by H, whereas the thickness of the porous medium is δ. The pressure gradient is adjusted so that the averaged velocity is set to unity. The numerical solution to this problem has been obtained by continuation methods using software AUTO07P [15]. The channel height and the extension of the porous medium are set to $H = 1$ and $\delta = 0.5$, respectively, so that the fluid and porous regions have comparable sizes. The homogeneous porosity was set to $\varepsilon_H = 0.41$ which is a typically reported value for packed beds [18].

As Δ is a crucial variable for the computation of the appropriate boundary conditions for the equivalent TDA problem, we carefully adjusted the constant b by considering the numerical solutions to the GTE equations (1). An example is shown in figure 2 for $Da = 10^{-4}$, $\varepsilon_H = 0.41$ and $b = 20$. The upper boundary of the interfacial region may be evaluated as the location of the maximum of the shear rate u_y, i.e. $y = 0.082$, which gives $\Delta \approx 1.64/b$. Hereinafter, we set $b = 2/\Delta$, thus a slightly larger evaluation of Δ, such that $\varepsilon(-\Delta)$ and $\kappa(-\Delta)$ depart from their constant values in the homogeneous porous region, ε_H and Da, by a relative distance of only 3×10^{-3}.

Modifying the representation of the continuous variations of the porosity and permeability in the interfacial region has a significant but weak influence on the ODA solution. We compare in figure 3 the solutions to the GTE equations (1) with the error-function representation (47) and with a hyperbolic-tangent representation

$$\varepsilon(y) = \frac{1}{2}\left[1 + \varepsilon_H + (1-\varepsilon_H)\tanh\,(b_1 y)\right], \quad \frac{1}{\kappa(y)} = \frac{1}{2Da}\left[1 - \tanh(b_1 y)\right] \quad \text{with} \quad b_1 = \sqrt{\pi}\ln 4 \tag{48}$$

where the constant b_1 has been adjusted such that the global friction exerted by the porous matrix on the flow may be equivalent, i.e. $\int_0^\infty \mathrm{erf}(2y)dy = \int_0^\infty \tanh(b_1 y)dy$.

Figure 4 compares the solution to GTE equations (1) with and without the second Brinkman corrections for $Da = 10^{-4}$ and different values of the ratio $a = \Delta/\delta_B$ of the thickness of the interfacial region to the

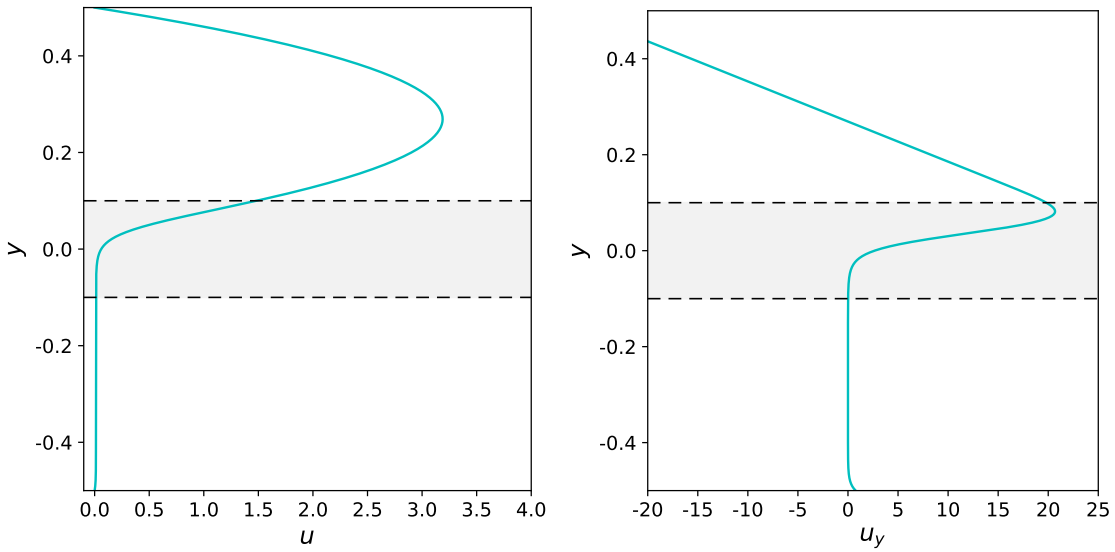

(a) velocity profile u

(b) shear rate distribution u_y

Figure 2: ODA solution to GTE (1) with error-function distributions (47) of porosity and permeability, $Da = 10^{-4}$ and $\varepsilon_H = 0.41$ and $b = 20$. The shaded band materializes the interfacial region defined by $\Delta = 2/b$.

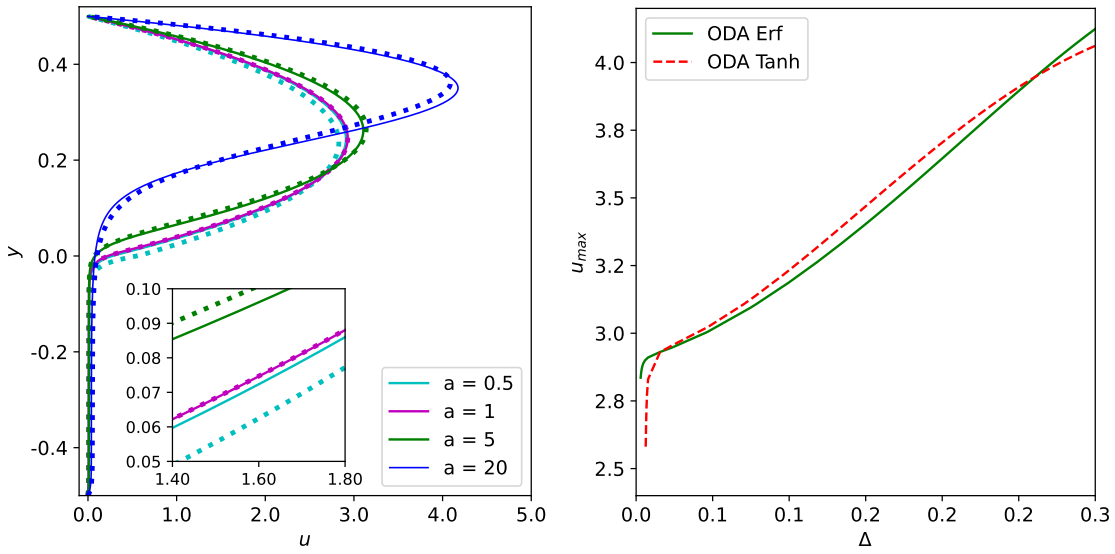

(a)

(b)

Figure 3: Comparison of ODA solutions with error-function distributions (47) of porosity and permeability (solid line), and hyperbolic-tangent distributions (48) (dashed lines) for different values of the ratio a of the interfacial region thickness Δ to the Brinkman penetration depth δ_B. Left: comparison of the velocity profiles; right: comparison of the maximum velocity $u_{\max}$ as a function of Δ. $Da = 10^{-4}$ and $\varepsilon_H = 0.41$.

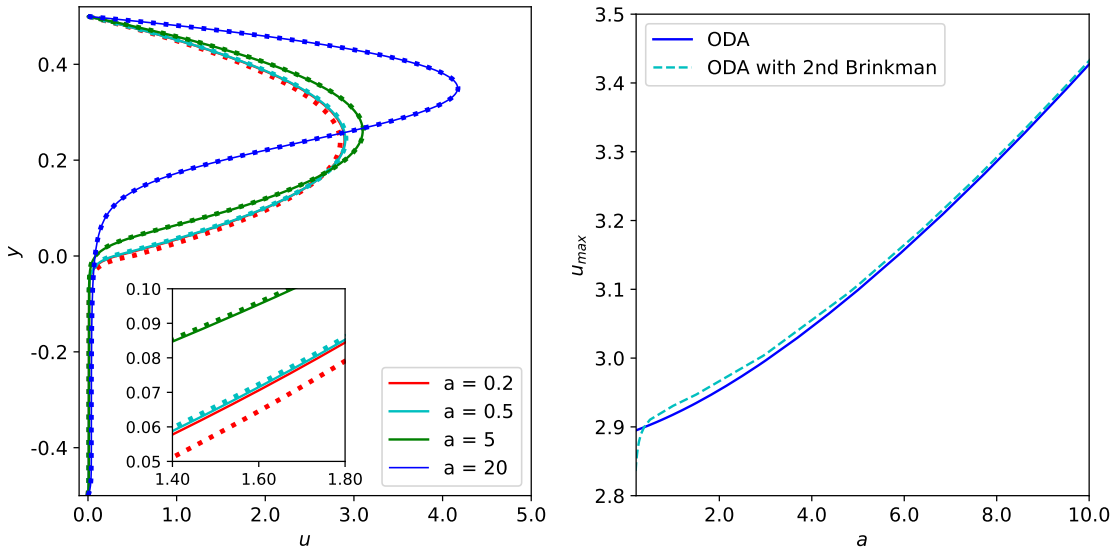

(a) (b)

Figure 4: Comparison of ODA solutions with (dotted line) and without (solid line) second-order Brinkman corrections for different values of the ratio a of the thickness of the interfacial region to the Brinkman penetration depth. Left: comparison of the velocity profiles; right: comparison of the maximum velocity $u_{\max}$ as functions of a. $Da = 10^{-4}$ and $\varepsilon_H = 0.41$.

Brinkman penetration depth. Since the first-order correction is of the order $O(\delta_B^{-2})$ and the second-order corrections are of the order $O(\Delta\delta_B)$, we expect the second-order Brinkman terms to be negligible at large values of a. Our computations confirm that second-order Brinkman corrections affect only weakly the ODA solution whenever a is larger than 0.5. Our findings suggest that neglecting the second-order Brinkman corrections is a valid simplification. Though, in agreement with Hernandez-Rodriguez *et al.* [20], we observe that the difference between the ODA solutions with and without these terms decreases only slowly with a.

We also observe that the velocity of the fluid at the inferior limit of the interfacial region, $u(y = -\Delta)$, departs from the seepage velocity $-Da\, p_x$ by a relative value which is inferior to 10 % whenever a is larger than 5 and for the tested range of porosities $\varepsilon_H \in [0.2, 0.8]$. We thus conclude that the Brinkman diffusion sub-layer can be assumed to be entirely contained within the interfacial region for $a > 5$, which justifies the derivation of the DTR model (37) in the thick-interface limit. Besides, for $a > 2$, the velocity in the porous region remains small as $u(y = -\Delta)$ is smaller than two times the seepage velocity $-Da\, p_x$, which justifies the use of the Darcy equations (4) and the DTR model (37) for $2 < a < 5$, even if the Brinkman sub-layer is not entirely contained within the interfacial region in that case.

We next compute the solutions to the TDA problem using the boundary conditions we have derived in section 2.2. Accuracy is assessed by comparisons to the reference ODA solutions in the fluid and porous outer regions, as TDA and ODA problems differ in the interfacial region.

Figure 5 compares the solutions to the TDA and ODA approaches as a is varied. The thickness of the interfacial region is maintained as $\Delta = 0.01$ by adjusting the Darcy number for ease of comparison. For all tested values of the parameter a, an excellent agreement of the TDA and ODA solutions is observed outside the interfacial region. At $a = 0.5$, the ODA solution presents large deviations of the velocity profile in the porous medium from the Darcy seepage velocity, which demonstrates that the Brinkman sub-layer is not contained within the interfacial region in that case. Panel a compares the solution of the GTE equations (1) to the TDA solution, where the flow in the porous layer is modelled by the Darcy-Brinkman law (3) and applying the jump boundary conditions (29) at the middle of the interfacial region ($\xi = 0$). An excellent agreement is found. In particular, the maximum velocity of the flow is accurately captured. Similar excellent agreements are observed at $a = 1.5$ (panel b) and $a = 3$ (panel c) where the

location of the dividing interface is adjusted with formula (32) so as to approach a near zero velocity at this interface. However, the solution to the Darcy-Brinkman equation (3) presents large deviations from the nearly constant velocity profile of the ODA solution in the vicinity of dividing interface for $a = 3$. Instead, the solution to the TDA approach modelled by the Darcy equation (4) and the DTR boundary conditions (37) accurately capture the flow in the porous medium, with the exception of the Brinkman layer at the lower wall. However, a less convincing agreement is found with the ODA solution in the fluid layer than with the TDA approach modelled by the Darcy-Brinkman equation (3) and (29). At $a = 10$, the TDA approach is modelled by the Darcy equation (4) and the DTR boundary conditions (37) with (38) or (46). The expressions (38) of the coefficients of the DTR model provide the best result with a solution in the fluid layer, which nearly coincides with the ODA solution. Indeed, the derivation of the DTR model of interfacial momentum transfer presented in section 2.3 accounts for the Brinkman sub-layer in the interfacial region, whereas the derivation of this model presented in section 2.4 assumes only a Darcy flow.

So far, we have compared the ODA and TDA solutions for which the boundary conditions have been derived by solving the TDA governing equations in the interfacial region in section 2.2. These boundary conditions, either (29) or the DTR model (37) are considerably more complex than the jump boundary conditions derived in section 2.1. Following Angot *et al.* [3], one may neglect the thickness of the interfacial region and directly apply on the sharp interface at $y_i = 0$ the jump conditions (13), (16), (14) and (17). Using the Darcy-Brinkman equations (3), the result is compared to the ODA solution in figure 6 for $a = 0.5$ and $a = 10$ and the same parameter set as that in figure 5. Without surprise, the agreement to the ODA solution is less convincing than when the thickness of the interfacial region is accounted for.

We end this section by discussing the influence of the location of the dividing interface, as defined by the parameter ξ, on the accuracy of the TDA solution with respect to the ODA solution. In our approach, the location of the dividing interface is adjusted to correspond approximately to the cancelling of the velocity in the fluid side u^l. This choice reflects the fact that the velocity in the fluid layer is much larger than in the porous layer, so the accuracy of the TDA solution corresponds principally to its capacity to represent correctly the flow in the fluid layer.

The location at which the velocity in the fluid layer effectively cancels can be evaluated by fitting the ODA solution by a parabola in the fluid region. Figure 7 compares the relative location of the dividing interface ξ/a obtained by this procedure to the estimates (32), (36) and (45) for two values of the porosity, $\varepsilon_H = 0.41$ and $\varepsilon_H = 0.78$. The latter value is typical of metal foam, for instance. For both cases, a reasonable agreement is found. The estimate (32) used in the range $a \in [(1+\varepsilon_H)/2, 2]$ is particularly accurate. The estimates (32) and (45) presents the same trend as the parabolic fit to the ODA solution, whereas the estimate (36) shows a different trend. However, all three estimates converge to the same asymptote $\xi/a = (1-\varepsilon_H)/(1+\varepsilon_H)$ as a is increased.

3.2 Stagnation point

We extend the well-known solution of a viscous stagnation point on a solid wall [44] to the case of a porous one with suction. The porous medium extends from $y = -\delta$ to the fluid-porous boundary at $y = 0$, whereas the overlying fluid layer extends to $y = H$ with $H \gg \delta$ in order to mimic a plane irrotational flow impinging a wall. The flow is assumed to be potential far from the boundary, i.e., $u \approx x$, $v \approx -y + cst.$, $p \approx -\frac{x^2+y^2}{2} + cst.$. We introduce a suction velocity $v_s = -A\,Da$ at the bottom $y = -\delta$ of the porous medium. In this test case, the Darcy seepage velocity is oriented in neither normal nor tangential direction to the porous-fluid interface. Besides, $v_y \neq 0$ in the interfacial region will enable us to check the presence of pressure jumps and normal velocity. The length scale is adjusted to set the Reynolds number to unity without loss of generality.

Following Schlichting & Gersten [44], we introduce the ansatz:

$$u = x f'(y)\,, \qquad v = -f(y)\,, \qquad p = -\frac{x^2}{2} - g(y)\,, \tag{49}$$

which enables to reduce the resolution of the original 2D problem to a 1D one. Within the ODA approach,

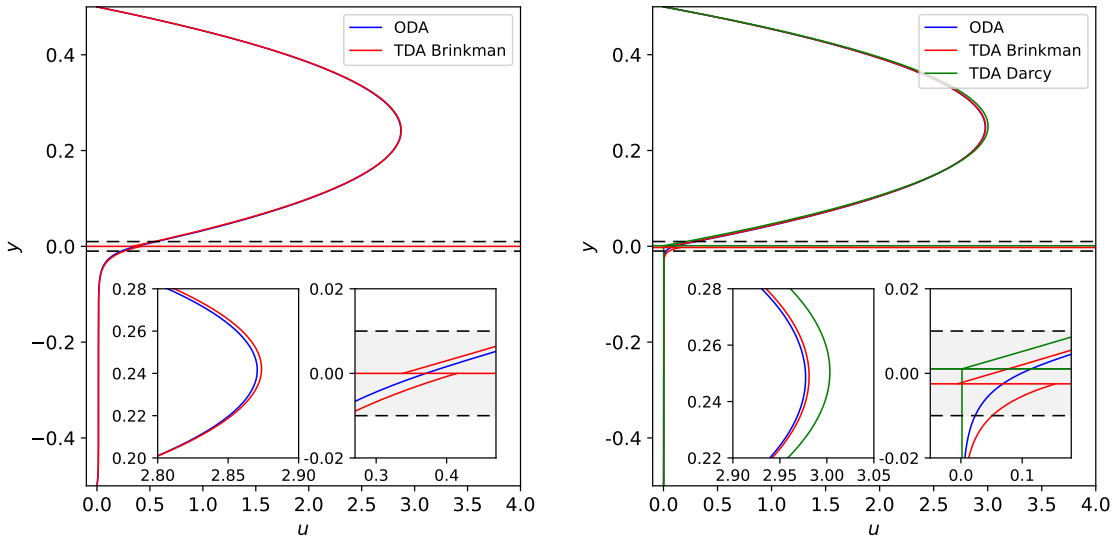

(a) $a = 0.5$

(b) $a = 1.5$

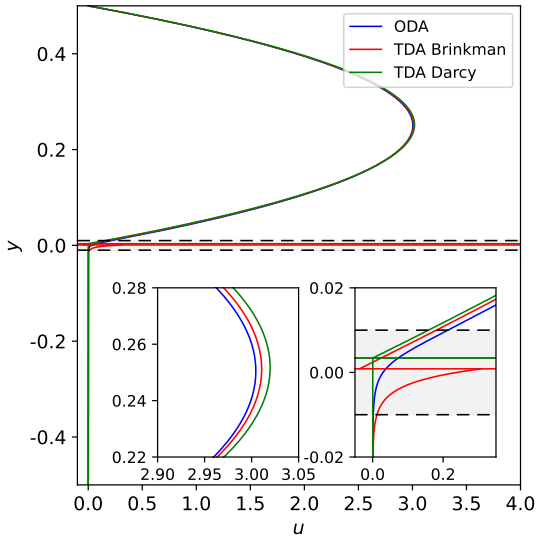

(c) $a = 3$

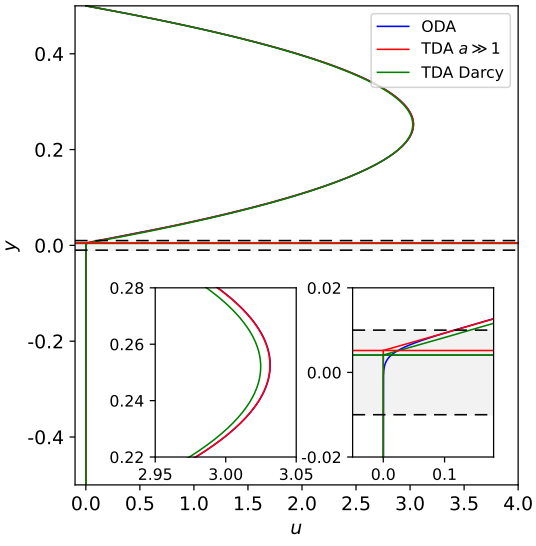

(d) $a = 10$

Figure 5: Comparison of ODA and TDA solutions for a constant thickness $\Delta = 0.01$ of the diffuse interface and different values of a. The Darcy number is adjusted to $Da = \varepsilon_H(\Delta/a)^2$ to mmaintain Δ constant.

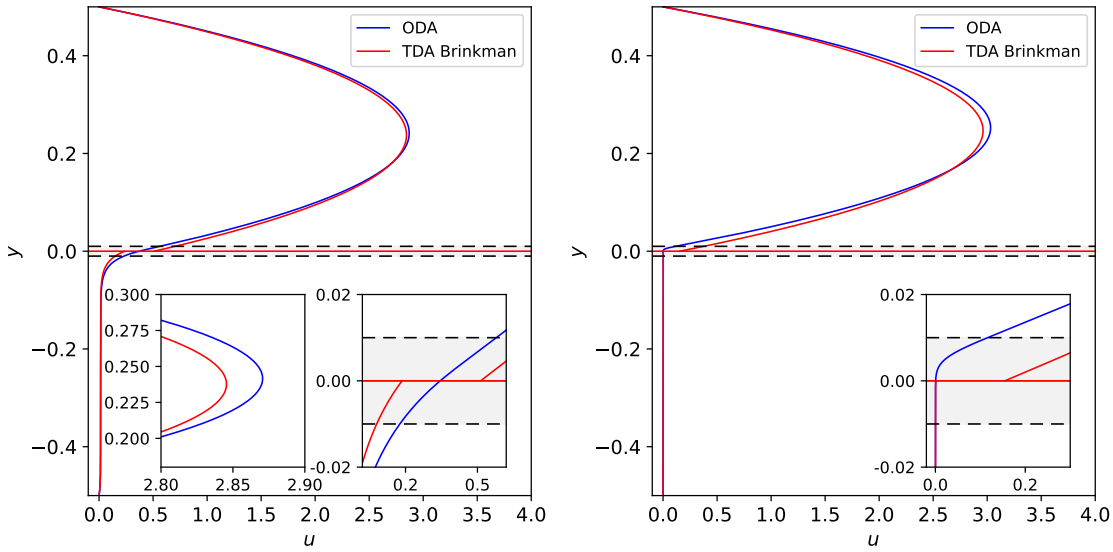

(a) (b)

Figure 6: Comparison of ODA and TDA solutions using the jump condition (13) and (16) when applied directly at the dividing interface $y = 0$. See the caption of figure 5.

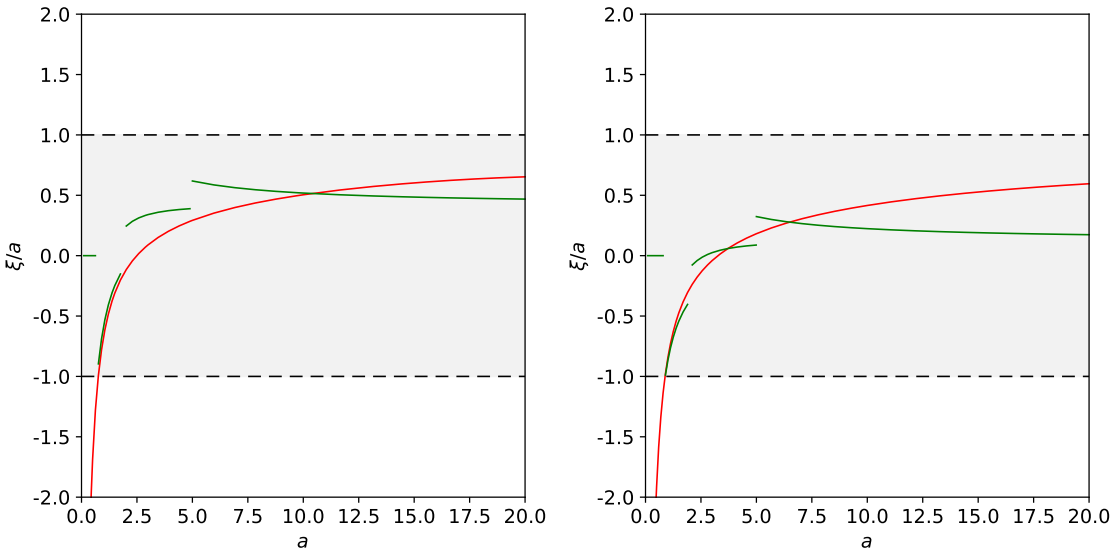

(a) $\varepsilon_H = 0.41$ (b) $\varepsilon_H = 0.78$

Figure 7: Estimation of the relative location ξ/a of the fluid-porous sharp interface from a parabolic fit of the ODA solution as compared to the formulae (32), (45) (36) for $Da = 10^{-4}$ and $\varepsilon_H = 0.41$ (left) and $\varepsilon_H = 0.78$ (right). See Table 1. The straight lines indicate the locations of the diffuse interface boundaries ($\xi = \pm a$).

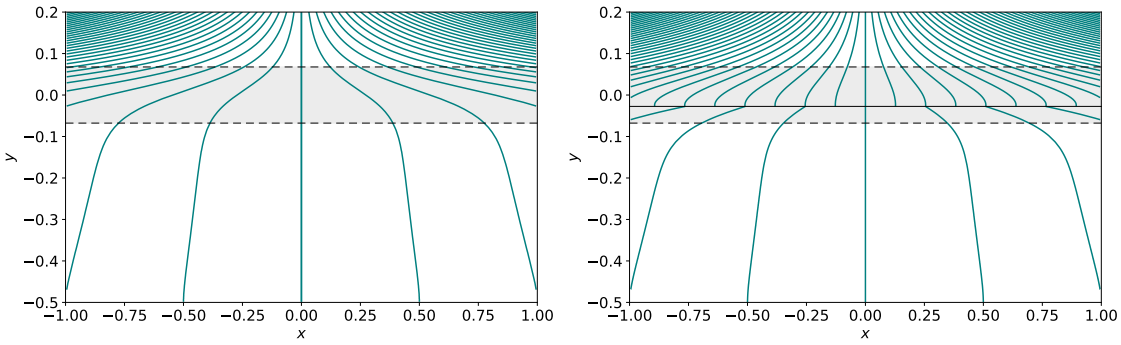

(a) ODA solution to (50)

(b) TDA solution to (52) with (29)

Figure 8: Streamlines in the porous region and in the vicinity of the diffuse interface (shaded regions) for the flow around a stagnation point with suction. $\delta = 0.5$, $Da = 10^{-3}$, $\varepsilon_H = 0.78$ and $a = 1.89$.

the system of equations to be solved thus reads

$$\frac{f'''}{\varepsilon} - \frac{f'}{\kappa} = \frac{1}{\varepsilon}\left[\frac{(f')^2 - ff''}{\varepsilon} + \frac{\varepsilon'}{\varepsilon^2} ff'\right] - 1\,, \tag{50a}$$

$$\frac{f''}{\varepsilon} - \frac{f}{\kappa} = \frac{1}{\varepsilon}\left[-\frac{ff'}{\varepsilon} + \frac{\varepsilon'}{\varepsilon^2} f^2\right] + g'\,, \tag{50b}$$

with the associated boundary conditions

$$f(-\delta) = A\,Da \quad , f'(-\delta) = g(-\delta) = 0\,, \quad f(H) = 1\,. \tag{51}$$

Within the TDA approach, the Darcy-Brinkman equations (3) yields

$$\frac{f^{p'''}}{\varepsilon_H} - \frac{f^{p'}}{Da} = \frac{(f^{p'})^2 - f^p f^{p''}}{\varepsilon_H^2} - 1\,, \quad \frac{f^{p''}}{\varepsilon_H} - \frac{f^p}{Da} = -\frac{f^p f^{p'}}{\varepsilon_H^2} + g^{p'}\,, \tag{52a}$$

$$f^{l'''} = (f^{l'})^2 - f^l f^{l''} - 1\,, \quad f^{l''} = -f^l f^{l'} + g^{l'}\,, \tag{52b}$$

which is closed by (51). Considering instead a Darcy flow within the porous medium, this system of equations reduces to (52b) with $f^p = Da(A+y)$ and $g^p = -\left(Ay + \frac{1}{2}y^2\right)$.

We solve again systems (50) and (52) by continuation methods using AUTO07P software for the set of parameters $\delta = 0.5$, $H = 10$ and $\varepsilon_H = 0.41$ or $\varepsilon_H = 0.78$. In the present test, the thickness of the interfacial region is evaluated using the Carman-Kozeny relation, which relates the typical grain size d of packed beds to their permeability

$$\kappa_H = \frac{\varepsilon_H^3 d^2}{180(1-\varepsilon_H)^2}\,. \tag{53}$$

Goharzadeh *et al.* [17] estimated the thickness of the diffuse interface to correspond to the size of a grain. We thus deduce from (53) an estimate for the dimensionless thickness of the interfacial region,

$$\Delta \approx 3\sqrt{5}\frac{1-\varepsilon_H}{\varepsilon_H}\delta_B\,, \tag{54}$$

which gives $\Delta \approx 9.6\delta_B$ for $\varepsilon_H = 0.41$ and $\Delta = 1.89\delta_B$ for $\varepsilon_H = 0.78$.

We first consider the case of a relatively thin interfacial region, for $Da = 10^{-3}$, $\varepsilon_H = 0.78$ and $a = 1.89$. Figure 8 illustrates the flow pattern and its symmetry around the stagnation point located at $x = 0$, in the porous region and at the diffuse interface. The streamlines are obtained from the expression $xf(y)$ of the stream function corresponding to the ODA solutions and to the TDA solution to the Darcy-Brinkman equation (52) with the jump boundary conditions (29). An excellent agreement is observed in the fluid and porous regions outside the diffuse interface.

Figure 9 further offers a direct comparison of the ODA solution to TDA solutions to the Darcy-Brinkman equation (52) with the jump boundary conditions (29), as well as to (52b) with the Darcy flow $f^p = Da(A+y)$ and $g^p = -\left(Ay + \frac{1}{2}y^2\right)$ and the DTR model (37) with (46). The Darcy-Brinkman equation with the jump conditions (29) predicts the velocity field ($u \propto f'$ and $v \propto f$) satisfactorily, even if the normal velocity in the fluid layer presents some discrepancies with the ODA solution. The velocity in the porous layer in the vicinity of the dividing interface is also somewhat overestimated. The solution to the TDA approach assuming a Darcy flow in the porous medium and using the DTR transfer model also performs satisfactorily. In particular, in both cases, the TDA approach reproduces accurately the pressure distribution within the flow represented by the function g, as well as the jump of tangential shear stress $u_y \propto f''$ across the interfacial region. Note that both (29) and (37) predict a positive jump of the pressure at the dividing interface, $p^l|_i - p^p|_i > 0$.

We next consider $Da = 10^{-4}$ and a porosity $\varepsilon_H = 0.41$, representative of packed beds, for which the Carman-Kozeny relation gives an estimate of the interfacial thickness corresponding to a relatively large value of $a = 9.6$. This time we compare the solution to the TDA with a Darcy flow $f^p = Da(A+y)$ and $g^p = -\left(Ay + \frac{1}{2}y^2\right)$ and the DTR model (37) with (38) or (46) to the reference solution to the ODA equations (50). An excellent agreement is observed either for the coefficient expressions (38) obtained in the limit $e^a \gg 1$ or the expressions (46) obtained considering a Darcy flow in the interfacial region. As for the parallel flow considered in § 3.1, the solution to the ODA approach predicts a velocity field in the homogeneous porous region ($y < -\Delta$) which remains close to the seepage velocity $-Da\nabla p$. We thus conclude that the assumption of a Brinkman sub-layer entirely contained in the interfacial region is again justified. The DTR model, either with (38) or (46), predicts a location of the dividing interface above the centre of the interfacial region ($\xi > 0$) in close agreement with the coordinate at which the velocity predicted by the ODA solution departs from the seepage Darcy velocity. The pressure jump $p^l|_i - p^p|_i$ is then negative. A situation which is inverted with respect to the case $\varepsilon_H = 0.78$ ($\xi < 0$ and $p^l|_i - p^p|_i > 0$), and is a direct consequence of the proportionality of the resistance coefficient F with ξ.

4 Concluding Remarks

The present investigation has considered a long-standing challenge to accurately describe and model the transport phenomena in a fluid-porous medium system and the transitional region between the two domains responsible for interfacial mass and momentum transfer. Our starting point is the GTE equations (1) as a valid macroscopic description of the momentum transfer at the fluid-porous interface [20]. Following Angot *et al.* [3], we have integrated the GTE equations across the interfacial region to obtain jump boundary conditions for the speed, pressure and shear stresses. Our derivation completes the work of Angot et al. by taking into account the variations of the normal velocity ($v_y \neq 0$), which yields a jump condition (16) for the normal velocity instead of the continuity condition postulated by Angot *et al.* [3], Ochoa-Tapia & Whitaker [39].

Within the framework of TDA, the jump conditions across the interfacial regions are rewritten at the fictitious dividing interface separating the homogeneous and isotropic porous medium and the fluid layer by solving the creeping flow in the interfacial region. Two parameters are identified, namely, the Brinkman penetration depth ($\delta_B = \sqrt{Da/\varepsilon_H}$) and the ratio of the transitional thickness to the Brinkman penetration depth ($a = \Delta/\delta_B$), which facilitated the derivation of the effective homogenized boundary conditions with coefficients expressed explicitly in terms of these two parameters. For a porous medium with given porosity, the coefficients in the boundary conditions account for the details about the diffusive transport into the porous medium across the interface and the frictional force generated by the Darcy seepage velocity that provides resistance to the imposed shear from the fluid region. The jump conditions are imposed on a fictive interface whose location within the transitional region can be specified in terms of another parameter (ξ) that depends on the parameters δ_B and a. The exact location of the interface may be decided by requiring that the obtained TDA solutions match very closely with the corresponding ODA solutions.

This study proposes three different formulations depending on the parameter a. When $a < 2$, the Darcy-Brinkman equations (3) are closed by the jump conditions (29) for the velocity, shear rate and pressure distribution. For $a > 2$, two similar sets of equations are derived, either by considering the limit $e^a \gg 1$ or by assuming the Darcy equation to be valid within the interfacial region. This formulation is based on the

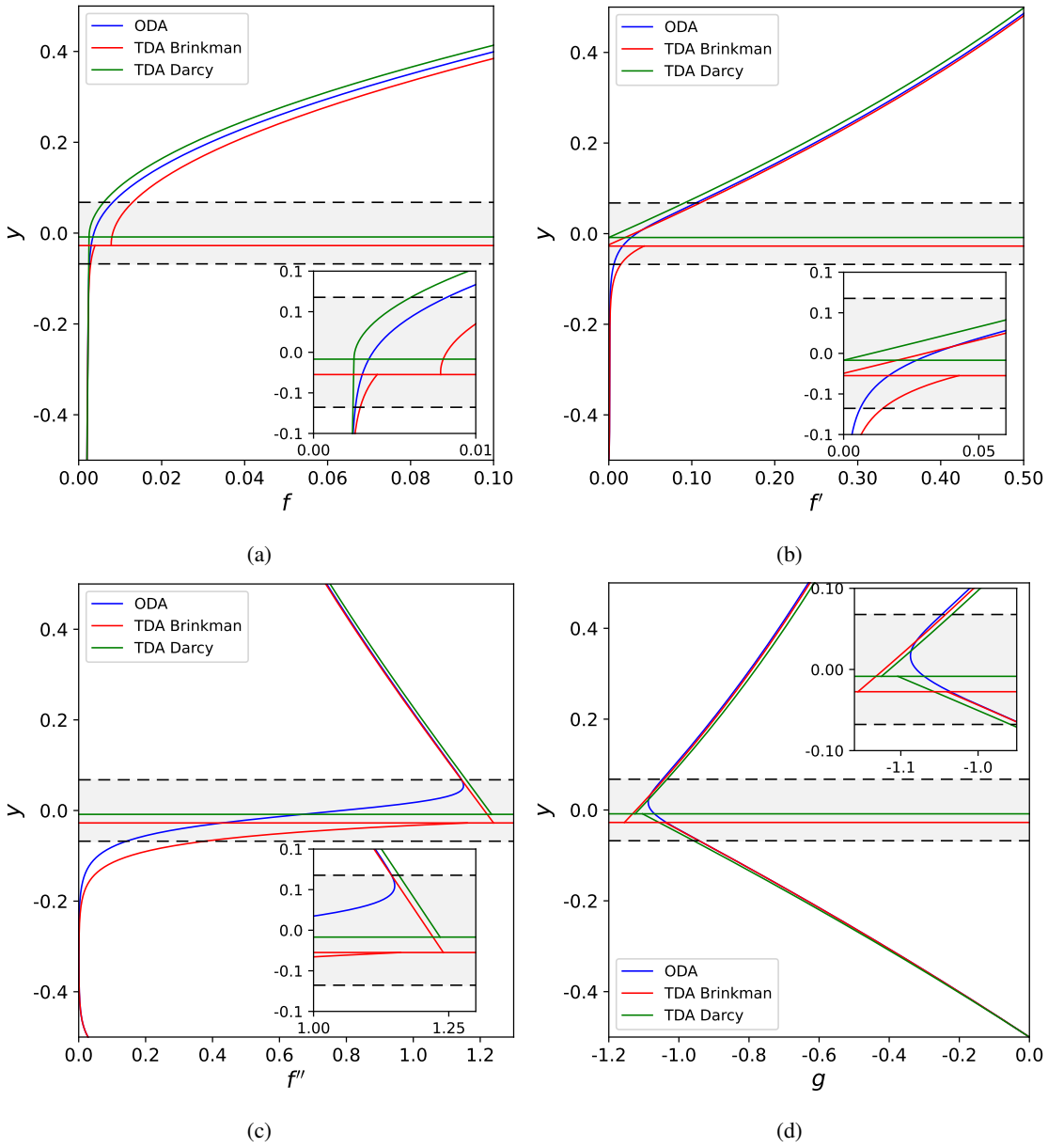

Figure 9: Comparison of ODA solution to (50), labelled 'ODA', with the TDA solution to (52) and (29), labelled 'TDA Brinkman', and with the TDA solution to (52b) and (37) with (46), labelled 'TDA Darcy'. ($Da = 10^{-3}$, $\varepsilon_H = 0.78$, $a = 1.89$ and $A = 2$).

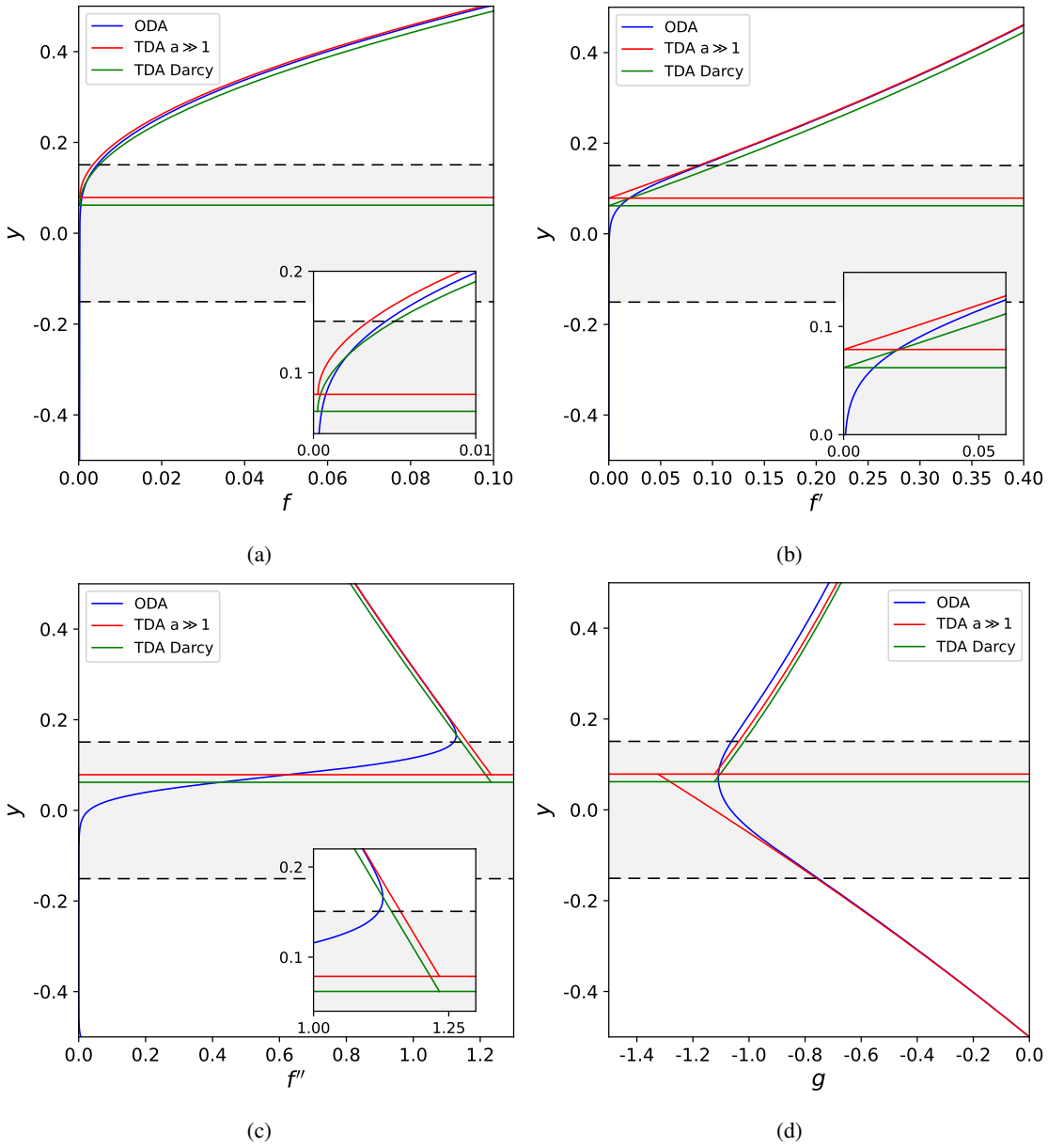

Figure 10: Comparison of ODA solution to (50), labelled 'ODA', with the TDA solutions to (52b) and the DTR model with (38), labelled 'TDA $a \gg 1$', and (46), labelled 'TDA Darcy'. ($Da = 10^{-4}$, $\varepsilon_H = 0.41$, $a = 9.7$ and $A = 2$).

consideration that the Brinkman sub-layer is contained within the interfacial region, which implies that the appropriate governing equation is the Darcy law in this case.

It is worth mentioning that these sets of boundary conditions resemble the slip-transpiration-resistance (STR) model (34) proposed by Lācis *et al.* [29]. The choice of the location of the sharp interface determines the sign of the resistance coefficient F, which can be determined independently of the choice of quadrature rules (see Appendix B). In this study, we choose to locate the fictitious dividing interface at a location where the fluid-side tangential velocity essentially vanishes ($u^l|_i = O(\Delta^2)$) and propose to replace the B-J slip condition by the continuity of the tangential velocity. As a result, a Dirichlet-transpiration-resistance (DTR) model (37) is proposed. The different obtained formulations and the range of the parameter a at which we propose to apply them are summarized in Table 1.

The derived boundary conditions have been tested by comparing the TDA solutions obtained with these boundary conditions and the corresponding ODA solutions for the following test problems: channel flow and stagnation point flow on a porous wall with suction. The satisfactory agreement of the solutions from the two approaches enhances our confidence that the proposed set of boundary conditions accurately captures the transport phenomena across the fictive sharp interface.

Our formulation is explicit with respect to a few geometrical parameters, which are easy to estimate in practice, and, therefore, can be easily implemented. This study is a first attempt towards a coherent mass and momentum model that complements the available models within the framework of TDA [3, 29]. The proposed model presents a pathway for extending the study to multiphase flows involving fluid-porous domains and multi-scale flow problems. Further, an extension of the study to include anisotropy of the porous medium, higher dimensional flow, and inhomogeneous porous layers is feasible and may require a higher order description in terms of the interfacial thickness Δ. The investigations on these and other relevant applications are in progress.

Acknowledgements

SM thanks Vellore Institute of Technology, Vellore, India, for providing *'VIT SEED Grant - RGEMS Fund (SG20220087)'* for carrying out this research work.

Declaration of Interests

The authors report no conflict of interest.

A Influence of the integration rule on the TDA boundary conditions

In this section, we discuss the influence of the choice of the numerical quadrature rule on the jump conditions across the interfacial region and the momentum transfer model for the TDA with two examples. We limit ourselves to parallel flows (i.e. $v_y = 0$) for simplicity. We show that the choice of the quadrature rule must ensure balanced jump conditions across the diffuse interfacial region in order to yield usable boundary conditions within the TDA approach.

A.1 Quadrature rule of a product

Using (9), we can write the quadrature

$$\int_a^b f(x)g(x)dx \approx \frac{h}{4}[f(a)+f(b)][g(a)+g(b)]\,, \tag{55}$$

which gives

$$\int_{-\Delta}^{\Delta} \frac{u}{\kappa}dy \approx \frac{1}{2\Delta}\int_{-\Delta}^{\Delta}\frac{1}{\kappa}dy\int_{-\Delta}^{\Delta}udy \approx \frac{1}{2Da}\left(u|_{\Delta}+u|_{-\Delta}\right) \tag{56}$$

and

$$\int_{-\Delta}^{\Delta} \frac{u_y}{\varepsilon} dy \approx \frac{1+\varepsilon_H}{4\varepsilon_H} \left(u_y|_{\Delta} + u_y|_{-\Delta} \right) \tag{57}$$

With this choice of a quadrature rule, the jump conditions connecting the fluid and porous regions within the ODA approach then reads for a parallel flow ($v_y = 0$)

$$\begin{aligned} \frac{1+\varepsilon_H}{2\varepsilon_H} \left(u_y|_{\Delta} - u_y|_{-\Delta} \right) &= \frac{\Delta}{2Da} \left(u|_{\Delta} + u|_{-\Delta} \right), & \text{(58a)} \\ u|_{\Delta} - u|_{-\Delta} &= \Delta \left(u_y|_{\Delta} + u_y|_{-\Delta} \right). & \text{(58b)} \end{aligned}$$

We note that balancing the terms of the tangential stress jump (58a) implies that $u|_{\Delta} = O(Da)$ since $u|_{-\Delta} = O(Da/\varepsilon_H)$. From (58), the following boundary conditions for the TDA problem are derived

$$\begin{aligned} (1+\varepsilon_H + a\xi - a^2) u_y^l|_i - \left[(1+\varepsilon_H)C - aS \right] u_y^p|_i &= \frac{a}{\delta_B} u^l|_i - \frac{(1+\varepsilon_H)S - aC}{\delta_B} u^p|_i, & \text{(59a)} \\ u^l|_i - (C - aS)\, u^p|_i &= -(S - aC)\delta_B u_y^p|_i. & \text{(59b)} \end{aligned}$$

In the limit of a thick interfacial region $e^a \gg 1$, this gives

$$u_y^l|_i = -\frac{(a-1)^2 + \varepsilon_H}{\delta_B (a-1)(a^2 - 1 - \varepsilon_H) - \xi \left[(a-1)^2 + \varepsilon_H \right]} u^l|_i. \tag{60}$$

which can be rewritten as a no-slip boundary condition at an effective sharp interface located at $y_i = \delta_B (a-1)(a^2-1-\varepsilon_H)/[(a-1)^2+\varepsilon_H] \approx a\delta_B = \Delta$, hence at the upper limit of the diffuse interfacial region. This is consistent with the estimate $u|_{\Delta} = O(Da) \ll 1$, which is necessary to balance the tangential shear jump (58a). Therefore, the quadrature rule (55) leads to un underestimation of the flow within the interfacial region.

A.2 Generalization of the trapezoidal rule

The trapezoidal quadrature rule can be generalized with the exact formula:

$$\begin{aligned} \int_a^b f(x)dx &= \frac{h}{2}[f(a)+f(b)] + \frac{h^2}{4}[f'(a) - f'(b)] + \frac{h^3}{12}[f''(a) + f''(b)] + \frac{h^4}{48}[f'''(a) - f'''(b)] \\ &\quad + \ldots + \frac{h^n}{2n!}[f^{(n)}(a) + (-1)^n f^{(n)}(b)] + \ldots \end{aligned} \tag{61}$$

Denoting by $\partial_{y^n} u$ the nth derivative of u with respect to y, we note that $\partial_{y^n}(u/\kappa)|_{\Delta} \approx 0$, $\partial_{y^{2n}}(u/\kappa)|_{-\Delta} \approx \delta_B^{-2n} u|_{-\Delta}$ and $\partial_{y^{2n+1}}(u/\kappa)|_{-\Delta} \approx \delta_B^{-2n} u_y|_{-\Delta}$. Summing the different series, we obtain after some algebra

$$\int_{-\Delta}^{\Delta} \frac{u}{\kappa} dy \approx \frac{\bar{C}\bar{S}}{\varepsilon_H \delta_B} u|_{-\Delta} + \frac{\bar{C}^2 - 1}{\varepsilon_H} u_y|_{-\Delta} \tag{62}$$

where $\bar{C} = \cosh a$ and $\bar{S} = \sinh a$. We have similarly

$$\int_{-\Delta}^{\Delta} \frac{u_y}{\varepsilon} dy \approx a\delta_B u_y|_{\Delta} + \frac{\delta_B \bar{C}\bar{S}}{\varepsilon_H} u_y|_{-\Delta} + \frac{\bar{C}^2 - 1}{\varepsilon_H} u|_{-\Delta} \tag{63}$$

We thus obtain the jump conditions

$$\begin{aligned} \frac{1+\varepsilon_H}{2\varepsilon_H} \left(u_y|_{\Delta} - u_y|_{-\Delta} \right) &= \frac{\bar{C}\bar{S}}{\varepsilon_H \delta_B} u|_{-\Delta} + \frac{\bar{C}^2 - 1}{\varepsilon_H} u_y|_{-\Delta}, & \text{(64a)} \\ \frac{1+\varepsilon_H}{2\varepsilon_H} \left(u|_{\Delta} - u|_{-\Delta} \right) &= a\delta_B u_y|_{\Delta} + \delta_B \frac{\bar{C}\bar{S}}{\varepsilon_H} u_y|_{-\Delta} + \frac{\bar{C}^2 - 1}{\varepsilon_H} u|_{-\Delta}, & \text{(64b)} \end{aligned}$$

from which we derive the following boundary conditions at $y = \xi a$ for the TDA problem:

$$(1+\varepsilon_H)u_y^l|_i - \left[(2\bar{C}-1+\varepsilon_H)C - 2\bar{C}\bar{S}S\right] u_y^p|_i = \left[2\bar{C}\bar{S}C + (1-\varepsilon-2\bar{C}^2)S\right] \frac{u^p|_i}{\delta_B}, \tag{65a}$$

$$(1+\varepsilon_H)u^l|_i - \left[(2\bar{C}-1+\varepsilon_H)C - 2\bar{C}\bar{S}S\right] u^p|_i = \delta_B\left[a(\varepsilon_H-1)+\xi(1+\varepsilon_H)\right] u_y^l|_i + \delta_B\left[2\bar{C}\bar{S}C + (1-\varepsilon-2\bar{C}^2)S\right] u_y^p|_i \tag{65b}$$

In the limit of a thick diffuse interface, i.e. $e^a \gg 1$, the boundary conditions (65) give $u_y^p|_i \approx -u^p|_i/\delta_B$. Similarly, the jump conditions (64) yields $u_y|_{-\Delta} \approx -u|_{-\Delta}/\delta_B$. These estimates are obviously unphysical. They arise from the imbalance of the jump conditions (64) as $\bar{C}$ and $\bar{S}$ diverge to infinity in the limit $a \gg 1$. We, therefore, conclude that the quadrature rule (8) does not yield valid boundary conditions for the TDA approach.

B Determination of the resistance coefficient F

In this section, we determine the friction coefficient F in the pressure jump of the STR model (52a). We show that the expression of F is independent of the quadrature rule.

To this aim, we consider a parallel and steady flow normal to the fluid-porous interface, the generalized transport equations (1) yields $v = cst$ and $p_y = -v/\kappa$. As a consequence, the pressure in the liquid region is constant and equal to its value at the sharp interface location, $p = p^l|_i$, and

$$p = p^l|_i + v\int_y^\infty \frac{1}{\kappa} dy \tag{66}$$

Integrating the Darcy (4) or Darcy-Brinkman equation (3) similarly gives

$$p^p = p^p|_i - \frac{v}{Da}(y - y_i). \tag{67}$$

Requiring next that for $y \ll -\Delta$, $p = p^p$ then gives

$$p^l|_i - p^p|_i = v\left(\frac{y_i - y}{Da} + \int_\infty^y \frac{1}{\kappa} dy\right), \quad \text{for} \quad y \ll -\Delta. \tag{68}$$

For an evenly distributed permeability around the middle $y = 0$ of the interfacial region we have

$$\int_\infty^y \frac{1}{\kappa} dy = \frac{y}{Da}. \tag{69}$$

As a consequence, we obtain

$$p^l|_i - p^p|_i = v\frac{y_i}{Da} = -F\,v. \tag{70}$$

From this we deduce the expression of the friction coefficient F such that

$$F = -\frac{y_i}{Da} = -\frac{\xi}{\delta_B \varepsilon_H} \tag{71}$$

which corresponds to the expressions (38) and (46).

References

[1] ALAZMI, B. & VAFAI, K. 2001 Analysis of fluid flow and heat transfer interfacial conditions between a porous medium and a fluid layer. *International Journal of Heat and Mass Transfer* **44** (9), 1735–1749.

[2] ANGOT, PHILIPPE, BOYER, FRANCK & HUBERT, FLORENCE 2009 Asymptotic and numerical modelling of flows in fractured porous media. *ESAIM: Mathematical Modelling and Numerical Analysis* **43** (2), 239–275.

[3] ANGOT, PHILIPPE, GOYEAU, BENOÎT & OCHOA-TAPIA, J. ALBERTO 2017 Asymptotic modeling of transport phenomena at the interface between a fluid and a porous layer: Jump conditions. *Phys. Rev. E* **95** (6), 063302.

[4] ANGOT, PHILIPPE, GOYEAU, BENOÎT & OCHOA-TAPIA, J. ALBERTO 2021 A nonlinear asymptotic model for the inertial flow at a fluid-porous interface. *Advances in Water Resources* **149**, 103798.

[5] BASSER, HOSSEIN, RUDMAN, MURRAY & DALY, EDOARDO 2017 Sph modelling of multi-fluid lock-exchange over and within porous media. *Advances in water resources* **108**, 15–28.

[6] BEAVERS, GORDON S. & JOSEPH, DANIEL D. 1967 Boundary conditions at a naturally permeable wall. *Journal of Fluid Mechanics* **30** (1), 197–207.

[7] BOTTARO, ALESSANDRO 2019 Flow over natural or engineered surfaces: An adjoint homogenization perspective. *Journal of Fluid Mechanics* **877**, P1.

[8] BREUGEM, WIM-PAUL & BOERSMA, BENDIKS-JAN 2005 Direct numerical simulations of turbulent flow over a permeable wall using a direct and a continuum approach. *Physics of fluids* **17** (2).

[9] BRILLARD, ALAIN, AMRANI, JAMAL EL & JARROUDI, MUSTAPHA EL 2013 Derivation of a contact law between a free fluid and thin porous layers via asymptotic analysis methods. *Applicable Analysis* **92** (4), 665–689, arXiv: https://doi.org/10.1080/00036811.2011.632768.

[10] CARRARO, T., GOLL, C., MARCINIAK-CZOCHRA, A. & MIKELIĆ, A. 2013 Pressure jump interface law for the stokes–darcy coupling: confirmation by direct numerical simulations. *Journal of Fluid Mechanics* **732**, 510–536.

[11] CHANDESRIS, M. & JAMET, D. 2006 Boundary conditions at a planar fluid–porous interface for a Poiseuille flow. *International Journal of Heat and Mass Transfer* **49** (13), 2137–2150.

[12] CHANDESRIS, M. & JAMET, D. 2007 Boundary conditions at a fluid–porous interface: An a priori estimation of the stress jump coefficients. *International Journal of Heat and Mass Transfer* **50** (17), 3422–3436.

[13] CHANDESRIS, M. & JAMET, D. 2009 Jump Conditions and Surface-Excess Quantities at a Fluid/Porous Interface: A Multi-scale Approach. *Transp Porous Med* **78** (3), 419–438.

[14] CIMOLIN, F. & DISCACCIATI, M. 2013 Navier–stokes/forchheimer models for filtration through porous media. *Applied Numerical Mathematics* **72**, 205–224.

[15] DOEDEL, EUSEBIUS J., CHAMPNEYS, A. R., FAIRGRIEVE, THOMAS F., KUZNETSOV, YU. A., SANDSTEDE, BJÖRN & WANG, XIANJUN 2008 AUTO 97: Continuation And Bifurcation Software For Ordinary Differential Equations (with HomCont) .

[16] GAVRILOV, KONSTANTIN, ACCARY, GILBERT, MORVAN, DOMINIQUE, LYUBIMOV, DMITRY, MÉRADJI, SOFIANE & BESSONOV, OLEG 2011 Numerical Simulation of Coherent Structures over Plant Canopy. *Flow Turbulence Combust* **86** (1), 89–111.

[17] GOHARZADEH, AFSHIN, KHALILI, ARZHANG & JØRGENSEN, BO BARKER 2005 Transition layer thickness at a fluid-porous interface. *Physics of Fluids* **17** (5), 057102.

[18] GOHARZADEH, AFSHIN, SAIDI, ARASH, WANG, DIANCHANG, MERZKIRC, WOLFGANG & KHALIL, ARZHANG 2006 An experimental investigation of the brinkman layer thickness at a fluid-porous interface. In *IUTAM Symposium on One Hundred Years of Boundary Layer Research* (ed. G. E. A. Meier, K. R. Sreenivasan & H.-J. Heinemann), pp. 445–454. Dordrecht: Springer Netherlands.

[19] GOYEAU, B., LHUILLIER, D., GOBIN, D. & VELARDE, M. G. 2003 Momentum transport at a fluid–porous interface. *International Journal of Heat and Mass Transfer* **46** (21), 4071–4081.

[20] HERNANDEZ-RODRIGUEZ, ROEL, ANGOT, PHILIPPE, GOYEAU, BENOÎT & OCHOA-TAPIA, J. ALBERTO 2022 Momentum transport in the free fluid-porous medium transition layer: One-domain approach. *Chemical Engineering Science* **248**, 117111.

[21] HERNANDEZ-RODRIGUEZ, R, GOYEAU, B, ANGOT, P & OCHOA-TAPIA, JA 2020 Average velocity profile between a fluid layer and a porous medium: Brinkman boundary layer. *Revista Mexicana de Ingeniería Química* **19** (Sup 1), 495–520.

[22] HILL, ANTONY A. & STRAUGHAN, BRIAN 2008 Poiseuille flow in a fluid overlying a porous medium. *Journal of Fluid Mechanics* **603**, 137–149.

[23] HIRATA, S. C., GOYEAU, B. & GOBIN, D. 2009 Stability of Thermosolutal Natural Convection in Superposed Fluid and Porous Layers. *Transp Porous Med* **78** (3), 525–536.

[24] HOU, J. S., HOLMES, M. H., LAI, W. M. & MOW, V. C. 1989 Boundary Conditions at the Cartilage-Synovial Fluid Interface for Joint Lubrication and Theoretical Verifications. *Journal of Biomechanical Engineering* **111** (1), 78–87.

[25] HUSSONG, JEANETTE, BREUGEM, WIM-PAUL & WESTERWEEL, JERRY 2011 A continuum model for flow induced by metachronal coordination between beating cilia. *Journal of Fluid Mechanics* **684**, 137–162.

[26] JÄGER, WILLI & MIKELIĆ, ANDRO 2009 Modeling effective interface laws for transport phenomena between an unconfined fluid and a porous medium using homogenization. *Transport in Porous Media* **78**, 489–508.

[27] JIMÉNEZ BOLAÑOS, SILVIA & VERNESCU, BOGDAN 2017 Derivation of the Navier slip and slip length for viscous flows over a rough boundary. *Physics of Fluids* **29** (5), 057103.

[28] LĀCIS, UĞIS & BAGHERI, SHERVIN 2017 A framework for computing effective boundary conditions at the interface between free fluid and a porous medium. *Journal of Fluid Mechanics* **812**, 866–889.

[29] LĀCIS, UĞIS, SUDHAKAR, Y., PASCHE, SIMON & BAGHERI, SHERVIN 2020 Transfer of mass and momentum at rough and porous surfaces. *Journal of Fluid Mechanics* **884**, A21.

[30] LĀCIS, UĞIS, TAIRA, KUNIHIKO & BAGHERI, SHERVIN 2016 A stable fluid–structure-interaction solver for low-density rigid bodies using the immersed boundary projection method. *Journal of Computational Physics* **305**, 300–318.

[31] LEVY, THÉRÈSE & SANCHEZ-PALENCIA, ENRIQUE 1975 On boundary conditions for fluid flow in porous media. *International Journal of Engineering Science* **13** (11), 923–940.

[32] LIU, QIANLONG & PROPSPERETTI, ANREA 2011 Pressure-driven flow in a channel with porous walls. *Journal of Fluid Mechanics* **679**, 77–100.

[33] LYUBIMOVA, T., LEPIKHIN, A., PARSHAKOVA, YA. & TIUNOV, A. 2016 The risk of river pollution due to washout from contaminated floodplain water bodies during periods of high magnitude floods. *Journal of Hydrology* **534**, 579–589.

[34] MIKELIC, ANDRO & JÄGER, WILLI 2000 On the interface boundary condition of beavers, joseph, and saffman. *SIAM Journal on Applied Mathematics* **60** (4), 1111–1127.

[35] MOHAMMADI, A. & FLORYAN, J. M. 2013 Pressure losses in grooved channels. *Journal of Fluid Mechanics* **725**, 23–54.

[36] MORAD, MOHAMMAD REZA & KHALILI, ARZHANG 2009 Transition layer thickness in a fluid-porous medium of multi-sized spherical beads. *Exp Fluids* **46** (2), 323–330.

[37] NIELD, DONALD A, BEJAN, ADRIAN & OTHERS 2006 *Convection in porous media*, , vol. 3. Springer.

[38] OCHOA-TAPIA, J.ALBERTO & WHITAKER, STEPHEN 1995 Momentum transfer at the boundary between a porous medium and a homogeneous fluid—ii. comparison with experiment. *International Journal of Heat and Mass Transfer* **38** (14), 2647–2655.

[39] OCHOA-TAPIA, J. ALBERTO & WHITAKER, STEPHEN 1995 Momentum transfer at the boundary between a porous medium and a homogeneous fluid—I. Theoretical development. *International Journal of Heat and Mass Transfer* **38** (14), 2635–2646.

[40] RICHARDSON, S. 1971 A model for the boundary condition of a porous material. Part 2. *Journal of Fluid Mechanics* **49** (2), 327–336.

[41] ROSTI, MARCO E., CORTELEZZI, LUCA & QUADRIO, MAURIZIO 2015 Direct numerical simulation of turbulent channel flow over porous walls. *Journal of Fluid Mechanics* **784**, 396–442.

[42] SAFFMAN, P. G. 1971 On the Boundary Condition at the Surface of a Porous Medium. *Studies in Applied Mathematics* **50** (2), 93–101.

[43] SAHRAOUI, M. & KAVIANY, M. 1992 Slip and no-slip velocity boundary conditions at interface of porous, plain media. *International Journal of Heat and Mass Transfer* **35** (4), 927–943.

[44] SCHLICHTING, H. & GERSTEN, K. 2001 *Boundary-Layer Theory*. Springer Berlin Heidelberg.

[45] TAYLOR, GI 1971 A model for the boundary condition of a porous material. part 1. *Journal of Fluid Mechanics* **49** (2), 319–326.

[46] TERZIS, A., ZARIKOS, I., WEISHAUPT, K., YANG, G., CHU, X., HELMIG, R. & WEIGAND, B. 2019 Microscopic velocity field measurements inside a regular porous medium adjacent to a low Reynolds number channel flow. *Physics of Fluids* **31** (4), 042001.

[47] VALDÉS-PARADA, FRANCISCO J., AGUILAR-MADERA, CARLOS G., OCHOA-TAPIA, J. ALBERTO & GOYEAU, BENOÎT 2013 Velocity and stress jump conditions between a porous medium and a fluid. *Advances in Water Resources* **62**, 327–339.

[48] VALDÉS-PARADA, FRANCISCO J., ALBERTO OCHOA-TAPIA, J. & ALVAREZ-RAMIREZ, JOSE 2007 Diffusive mass transport in the fluid–porous medium inter-region: Closure problem solution for the one-domain approach. *Chemical Engineering Science* **62** (21), 6054–6068.

[49] VALDÉS-PARADA, FRANCISCO J., GOYEAU, BENOÎT & OCHOA-TAPIA, J. ALBERTO 2007 Jump momentum boundary condition at a fluid–porous dividing surface: Derivation of the closure problem. *Chemical Engineering Science* **62** (15), 4025–4039.

[50] VALDÉS-PARADA, F. J. & LASSEUX, D. 2021 Flow near porous media boundaries including inertia and slip: A one-domain approach. *Physics of Fluids* **33** (7), 073612.

[51] VALDÉS-PARADA, FRANCISCO J., GOYEAU, BENOÎT & ALBERTO OCHOA-TAPIA, J. 2006 Diffusive mass transfer between a microporous medium and an homogeneous fluid: Jump boundary conditions. *Chemical Engineering Science* **61** (5), 1692–1704.

[52] WOOD, BRIAN D., QUINTARD, MICHEL & WHITAKER, STEPHEN 2000 Jump conditions at non-uniform boundaries: the catalytic surface. *Chemical Engineering Science* **55** (22), 5231–5245.

[53] ZAMPOGNA, GIUSEPPE A. & BOTTARO, ALESSANDRO 2016 Fluid flow over and through a regular bundle of rigid fibres. *Journal of Fluid Mechanics* **792**, 5–35.

[54] ZAMPOGNA, GIUSEPPE A., MAGNAUDET, JACQUES & BOTTARO, ALESSANDRO 2019 Generalized slip condition over rough surfaces. *Journal of Fluid Mechanics* **858**, 407–436.

[55] ZHANG, QUAN & PROSPERETTI, ANDREA 2009 Pressure-driven flow in a two-dimensional channel with porous walls. *Journal of Fluid Mechanics* **631**, 1–21.